AD-A186 737 GROUP IIA METASTABLE COLLISION COMPLEXES: SPECTROSCOPY AND BEHAVIOR IN IN..(U) JOINT INST FOR LAB ASTROPHYSICS BOULDER CO J COOPER ET AL. 18 SEP 87 AFOSR-TR-87-1374 1/1

UNCLASSIFIED AFOSR-84-0027 F/G 7/2 NL

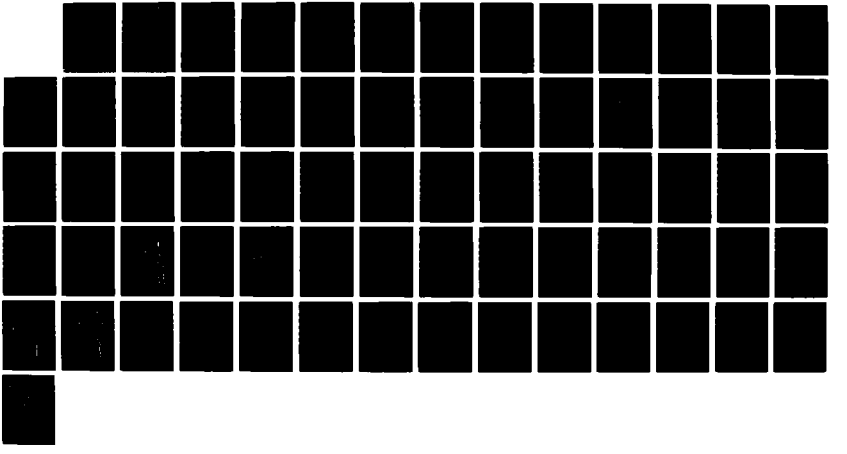

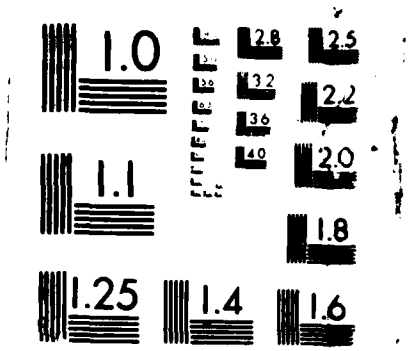

AD-A186 737

REPORT DOCUMENTATION PAGE

Unclassified	1b. RESTRICTIVE MARKINGS
2a. SECURITY CLASSIFICATION AUTHORITY	3. DISTRIBUTION/AVAILABILITY OF REPORT: Approved for public release; Distribution unlimited
2b. DECLASSIFICATION/DOWNGRADING SCHEDULE	
4. PERFORMING ORGANIZATION REPORT NUMBER(S)	5. MONITORING ORGANIZATION REPORT NUMBER(S): AFOSR-TR- 87-1374
6a. NAME OF PERFORMING ORGANIZATION: University of Colorado	6b. OFFICE SYMBOL (If applicable):
7a. NAME OF MONITORING ORGANIZATION: AFOSR/NC	
6c. ADDRESS (City, State and ZIP Code): Joint Institute for Laboratory Astrophysics, Boulder, CO 80309-0440	7b. ADDRESS (City, State and ZIP Code): Bldg 410, Bolling AFB DC 20332-6448
8a. NAME OF FUNDING/SPONSORING ORGANIZATION: AFOSR	8b. OFFICE SYMBOL (If applicable): NC
9. PROCUREMENT INSTRUMENT IDENTIFICATION NUMBER: AFOSR-84-0027	
8c. ADDRESS (City, State and ZIP Code): Bldg 410, Bolling AFB DC 20332-6448	10. SOURCE OF FUNDING NOS.

PROGRAM ELEMENT NO.	PROJECT NO.	TASK NO.	WORK UNIT NO.
61102F	2303	B1	

11. TITLE (Include Security Classification): Group IIA Metastable Collision Complexes: Spectroscopy and Behavior in Intense Radiation Fields

12. PERSONAL AUTHOR(S)

13a. TYPE OF REPORT	13b. TIME COVERED	14. DATE OF REPORT (Yr., Mo., Day)	15. PAGE COUNT
FINAL	FROM _____ TO _____		64

16. SUPPLEMENTARY NOTATION

17. COSATI CODES			18. SUBJECT TERMS (Continue on reverse if necessary and identify by block number)
FIELD	GROUP	SUB. GR.	Keywords: Slow Atomic Collisions, Chemical Lasers

19. ABSTRACT (Continue on reverse if necessary and identify by block number)

In this final report we describe work addressing the problems of collisional induced oscillator strength and energy transfer from metastable states in Group IIA alkaline earth metal atoms. We have investigated the quenching of CA 3PJ states when perturbed by rare was atom collisoions and found such quenching to be negligable. The CA 1D2 state, however shows considerable collisional induced effects. Calculations have been performed which show that collision cross-sections for transfer of electronic excitation may be switched from the low values typically associated with off-resonant processes to the high values associated with resonant processes by using a strong laser to bring dressed states in one atom in and out of resonance with bare states in another atom.

investigated

20. DISTRIBUTION/AVAILABILITY OF ABSTRACT	21. ABSTRACT SECURITY CLASSIFICATION
UNCLASSIFIED/UNLIMITED ☐ SAME AS RPT. ☒ DTIC USERS ☐	Unclassified

22a. NAME OF RESPONSIBLE INDIVIDUAL	22b. TELEPHONE NUMBER (Include Area Code)	22c. OFFICE SYMBOL
Dr Frank Wodarczyk	(202) 767-4963	NC

DD FORM 1473, 83 APR EDITION OF 1 JAN 73 IS OBSOLETE. SECURITY CLASSIFICATION OF THIS PAGE

Final Report **AFOSR-TR- 87-1374**

GROUP IIA METASTABLE COLLISION COMPLEXES: SPECTROSCOPY AND BEHAVIOR IN INTENSE RADIATION FIELDS

J. Cooper and J. Coutts

Joint Institute for Laboratory Astrophysics

National Bureau of Standards and University of Colorado

Boulder, Colorado 80309-0440

A final report of work performed for the U.S. Air Force under contract number AFOSR 84-0027, at the University of Colorado, of relevance to state-resolved chemistry, chemical lasers, and fundamental slow atom collision physics.

Abstract

In this final report we describe work addressing the problems of collisional induced oscillator strength and energy transfer from metastable states in group IIA alkaline earth metal atoms. We have investigated the quenching of Ca ^3P_J states when perturbed by rare gas atom collisions, and found such quenching to be negligible. The Ca $^1D_2$ state, however shows considerable collisional induced effects and we have made detailed measurements of collisionally induced absorption spectra. Collision induced absorption has been considered theoretically, with careful deliniation of intra- and inter-collisional interactions, and inter-collisional coherences.

Calculations have also been performed which show that collision cross sections for transfer of electronic excitation may be switched from the low values typically associated with off-resonant processes to the high values associated with resonant processes by using a strong laser to bring dressed states in one atom in and out of resonance with bare states in another atom.

Experimentally, the diffusion of tagged particles (specifically Ca^3P metastables) have been studied by a new technique which holds considerable potential for, at last, accurately studying transport in non-equilibrium situations.

Contents

		Page
1.	The relevance of this work to the Air Force	4
2.	Introduction	4
3.	Tagged particle diffusion	6
4.	An investigation into the effects of collisions on the ^3P_J manifold in calcium	12
5.	Modification of electronic excitation transfer collision cross sections with an ac Stark effect	18
6.	Theoretical investigations into collisionally induced absorption and emission	22
7.	Experiments on the calcium $^1D_2$ state - initial investigations	30
8.	Further investigations into the collisionally induced transition in calcium	40
9.	Conclusions and further work	44
10.	References	45
11.	Publications and conference abstracts	49
12.	The people involved in this contract	50

1. The relevance of this work to the Air Force

The Air Force has provided support in the fields relevant to short wavelength chemical lasers. To this end, investigation of the relevant cross sections are important to enable reasoned decisions to be made on the feasibility or otherwise of proposed chemical laser schemes. Electronically excited metastable species can be produced in various reaction schemes, and quenching processes and methods of manipulating excitation transfer collision cross sections affect the efficiency of the energy storage medium. Both modelling efforts and experimental demonstration schemes benefit enormously from an expanded data base of cross sections, and improvement in calculational techniques is worthwhile when the experimental situation is unresolved or inaccessible.

2. Introduction

This report describes work pertaining to the interaction of light with metastable group IIA species in a collisional environment. The contract has supported both theoretical and experimental work. The experimental program has focused on various forbidden lines in calcium, a convenient group IIA metal in terms of the ease of obtaining a calcium vapor in the laboratory. Our experiments have used diffusion controlled heated vapor cell technology for providing calcium atoms in a collisional environment, accessible to pulsed dye laser light. In such devices the interaction volume is frequently of small spatial extent - the observed volume is typically an excitation "pencil" of length of some 5 mm and diameter 1 mm. The natural lifetimes of metastable species are many orders of magnitude longer than the spontaneous lifetimes of allowed electric dipole transitions. Loss of experimental signal due to diffusion of excited species out of the observed volume can be a major

effect. Before the details of the collisional interactions of the metastable species could be probed, it proved necessary to conduct experiments to obtain information that could be used to define experimental regimes in which diffusion could be neglected. Such experiments are discussed in Sec. 3.

The information gleaned from tagged-particle diffusion experiments could be used to design simple but reliable experiments investigating the effect of collisions on spin forbidden electric dipole transitions. The $^1S_0 \rightarrow {}^3P_1$ transition in Ca I was chosen for investigation since some controversy existed in the literature on the value of the ^3P_J quenching rate constants, when rare gas atoms were used as quenchers. Thus our results could be compared directly to the results of others. We obtained a negligible quenching rate in the Ca Ar collision system, a result which can be attributed to the electrostatic nature of the collisional perturbation.

Electrostatic perturbations do not, to first order, affect the degree of LS coupling breakdown for isolated transitions. This work is described in Sec. 4.

The analogous metastable states in magnesium, the Mg ^3P manifold has received considerable attention as a potential chemical laser storage medium. The usefulness of such a storage medium depends in part on the ease of extraction of stored energy. One method of manipulating excitation transfer collision cross sections is described in Sec. 5. A strong laser tuned to an excited state transition in, e.g. a Sr atom, creates dressed states which may be placed into and out of resonance with the Mg $^3P_1$ state. Cross sections for excitation transfer can be switched from the low values associated with off-resonant processes to the high values associated with resonance phenomena. Typically cross sections can be enhanced by factors of order 10^3.

Although isolated spin-forbidden transitions are insignificantly altered to first order by electrostatic collisions, spin allowed transitions arising from higher order multipoles than electric dipole may indeed exhibit collisional enhancement of oscillator strength. The contract has supported theoretical work on the description of collisional induced effects on electric quadrupole transitions, with reference to the Ca $^1S_0 \rightarrow {}^1D_2$ transition. Here too, some experimental results have been reported in the literature. The major results of the theoretical investigation are described in Sec. 6.

In Sec. 7 we describe the experimental program we have undertaken to investigate collisional induced effects on the Ca $^1S_0 \rightarrow {}^1D_2$ transition. Using pump probe techniques we have obtained lineshape data for Ca/Ar and Ca/Kr and verified that in the regions of investigation each collisional induced absorption requires one collision and one photon for completion.

In Sec. 8 we extend the results of Sec. 7 to include Ca/He, Ca/Ne and Ca/Xe. In the case of Ca/Xe, in particular, an extensive sequence of improvements of the detection equipment was necessary.

In Sec. 9 we outline the conclusions that this work has allowed us to draw, and some ideas for future work that would be worthwhile. Section 11 indicates the extent to which work supported by this contract has been published and disseminated.

3. Tagged particle diffusion

The trial experiment discussed below arose in part because the metastable species that were the subject of this contract may diffuse long distances with respect to excitation volume dimensions before they decay spontaneously. The metastable species can be thought of as tagged particles, and the basic idea of this experiment is to produce a set of these tagged particles in a gas

using pulsed dye laser excitation and map out its evolution in space and time directly. The experiment, along with its analysis is rather crude, although it does give enough of a basis to design the further experiments on the interaction of metastable states with rare gas atoms. The experiment is similar in concept to the direct measurement of radiative transport as performed by Molander et al.[1]

The experiment is sketched in Fig. 3.1. A stainless steel cell was first evacuated and then charged with calcium metal in an argon atmosphere. The cell was heated to produce a vapor of calcium. In the experiments the cell temperature was 585°C producing a number density of $\sim 10^{13}$ cm^{-3} for the calcium. The argon density was always much larger than this, $\sim(10^{15}-10^{17})$ cm^{-3}. Two pulsed dye lasers were used to produce and probe calcium 4s4p $^3P_1$ metastables. The first laser pumped the ($^1S_0 \rightarrow {}^3P_1$ "forbidden") transition at $\lambda = 657.3$ nm. This produced a pencil of excitation along the center of the cell approximately 300 μm in diameter. The second laser was displaced spatially from the excitation region and delayed in time. This delay was achieved by timing the Q-switched pulses of the two Nd-YAG pump lasers. The second laser pumped atoms from the 4s4p $^3P_1$ to the 4s5s ^3S which then decay rapidly and emit radiation around 612 nm. This spontaneous emission was detected using a photomultiplier and recorded using a gated integrator linked to a Cromemco minicomputer. This 612 nm fluorescence is proportional to the density of the 4s4p $^3P_1$ atoms at the time and spatial position of the probe pulse. The profile of the excitation of $^3P_1$ atoms was recorded at several delays by scanning the second laser beam across the first to map out a spatial distribution of the "labelled" Ca atoms at fixed time delay.

The experiment essentially measures the joint probability density, $G(\vec{r},t;\vec{r}_0,0)$ for the excited Ca* atoms. This quantity gives the probability

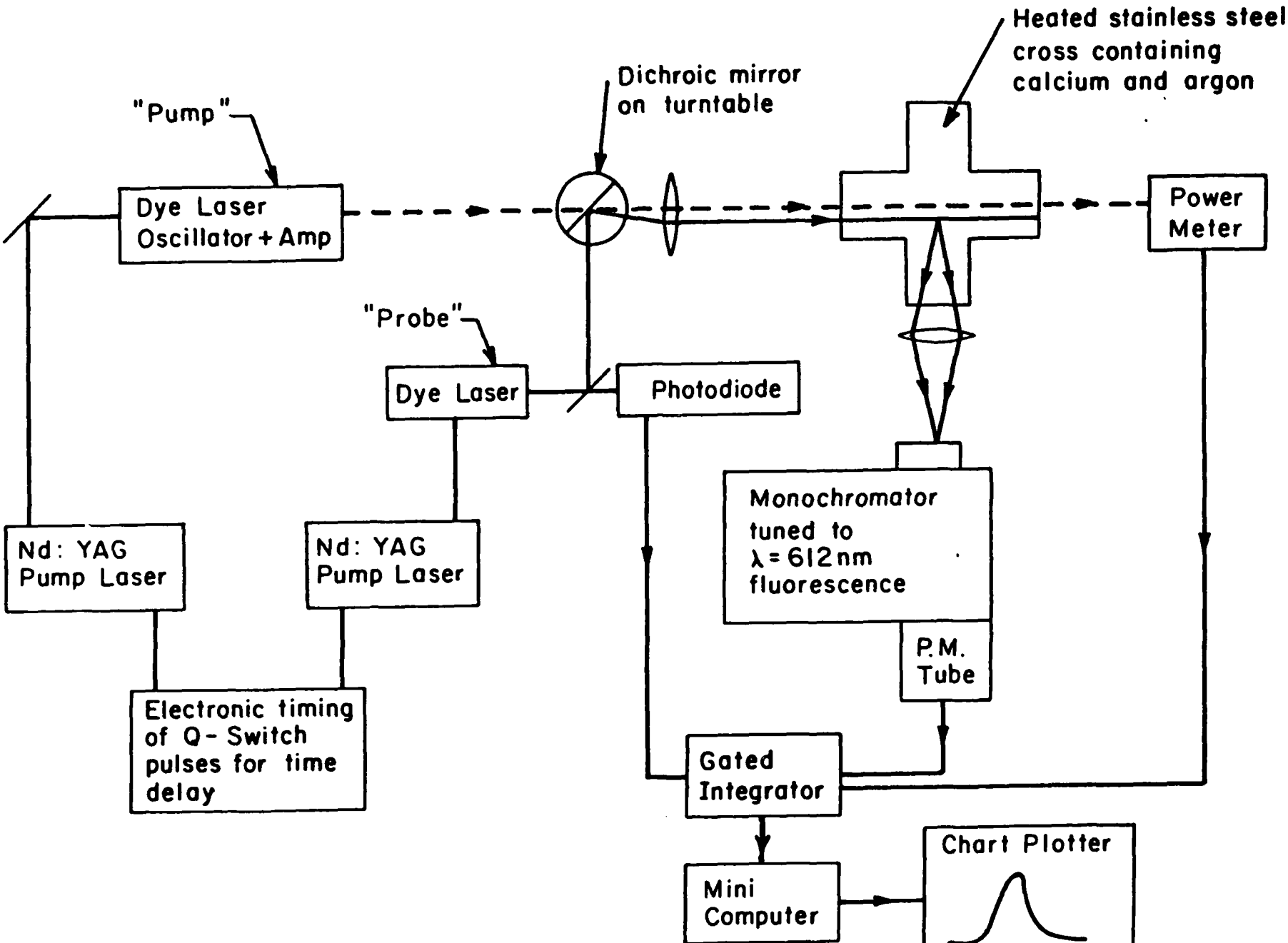

Figure 3.1 Schematic diagram of the experiment.

for detecting an excited Ca* atom at $(\vec{r},t)$, having created it at $(\vec{r}_0,t=0)$. Due to finite excitation and detection resolution the quantity observed is the spatial convolution of $G(\vec{r},t;\vec{r}_0,0)$ with two characteristic functions,

$$S(z,t) = \int d\vec{r}\, d\vec{r}_0\, I_z(\vec{r}) I_0(\vec{r}_0)\, G(\vec{r},t;\vec{r}_0,0) \quad . \tag{3.1}$$

Here $I_z(\vec{r})$ defines the long pencil-like probe beam profile, orthogonal to the z-axis and centered about the point, z. The probe beam profile can be measured by scanning a pinhole. The cross section of the initial excitation $I_0(\vec{r})$, can be thought of as approximately a circle of diameter $d \sim 300$ μm, whereas the effective length of the pencil is >1 cm. In general, $I_0(\vec{r}_0)$ can be determined experimentally to within a few percent, and it may be convenient to vary d for some purposes. The pumping times for the metastables is about 10 ns while their lifetime is about 1 ms due to fine structure changing collisions.[2] This defines the time scales for which Eq. (3.1) can be studied. The spatial resolution is limited by d, which could be made as small as ~10 μm with a spatially filtered pump laser. There are no limitations on the maximum values of z. These space and time scales are significantly different from those of neutron scattering or Brillouin light scattering experiments typically used to measure dynamic fluctuations in gases. In particular, the larger space and time scales open the possibility for study of nonequilibrium phenomena, as discussed below, that are difficult to observe with neutrons or light scattering.

The Green's function, $G(\vec{r},t;\vec{r}_0,0)$, is a Gaussian function of $|\vec{r}-\vec{r}_0|$ at both asymptotically short times (free streaming) and long times (diffusion). The primary characteristic feature of S(z,t) is therefore its width (at half maximum) as a function of time, $\xi(t)$, which describes the transition between kinetic and hydrodynamic stages for the transport of the Ca* atoms. Table I

Table 3.I. Experimental widths $\xi(t)$ of $S(z,t)$

p(torr)	t(ns)	ξ(μm)	t/t_0	$\alpha/D(\infty)t_0$
1	20	511 ± 5	0.048	0.001
	50	523 ± 9	0.119	0.037 ± 0.042
	100	520 ± 9	0.238	0.028 ± 0.042
	200	526 ± 23	0.476	0.046 ± 0.085
	350	607 ± 7	0.833	0.311 ± 0.039
4	40	480 ± 8	0.381	0.072
	100	480 ± 12	0.952	0.07 ± 0.89
	200	513 ± 8	1.905	1.58 ± 0.73
	350	531 ± 3	3.333	2.45 ± 0.50
10	20	465 ± 5	0.476	0.113
	100	470 ± 10	2.381	1.5 ± 4.1
	300	486 ± 10	7.143	5.9 ± 4.1
40	100	493 ± 7	9.524	
	350	500 ± 7	33.33	

shows the experimental conditions of pressure and time sampled and the associated widths, $\xi(t)$, observed.

A simple model that incorporates both short and long time limits is the Gaussian model,[3] for which $G(\vec{r},t;\vec{r}_0;0)$ obeys the usual diffusion equation but with a time-dependent diffusion coefficient

$$D(t) \equiv \frac{1}{3}\int_0^t d\tau \ \langle \vec{v}\cdot\vec{v}(\tau)\rangle \tag{3.2}$$

In this model, the width of $G(\vec{r},t;\vec{r}_0,0)$, is proportional to $(\alpha(t))^{1/2}$, where

$$\alpha(t) \equiv \int_0^t d\tau \ D(\tau) \tag{3.3}$$

The short-time (free streaming) behavior ($t/t_0 \ll 1$) is given by $\alpha(t) \to \frac{1}{6}\langle v^2\rangle t^2$; thus this model describes the short-time behavior of $G(\vec{r},t;\vec{r},0)$ exactly. In this limit the particles move freely and the distribution function obeys the following evolution rule:

$$f(\underline{r},\underline{v},t) = f(\underline{r}-\underline{v}t,\underline{v},0) \quad ,$$

and the behavior of the excited state number density $n(\underline{r},t) = \int d\underline{v}\ f(\underline{r};\underline{v};t)$ given by this rule agrees exactly with the Gaussian model.

In the long-time (diffusion) limit, $\alpha(t) \to D(\infty)t$. Therefore, the Gaussian model is exact for short times, and provides the diffusion limit for long times. It is also a good interpolation between these two limits.[4,5] The width of $S(z,t)$ depends, of course, on the form of G, the probe beam profile and the form of the initial distribution. To be precise, it is a convolution of these functions, as shown in Eq. (3.1). We approximate the spatial distribution for the pump and probe beams by Gaussian functions. After the convolution is taken over the initial distribution and probe beam profile, the relationship between the observed width, $\xi(t)$, and $\alpha(t)$ is simply

$$\xi^2(t) = \xi^2(0) + 16\ \ell n2\ \alpha(t) \quad , \tag{3.4}$$

where $\xi(0)$ is the initial excitation width plus the probe beam width added in quadrature. Thus, for small times the width is proportional to

$$\left(\frac{3\xi^2(0)}{8\ \ell n2} + v^2t^2\right)^{1/2}$$

and for long times is proportional to $\sqrt{Dt}$ (for $Dt >> \xi(0)$).

We have fitted the initial width $\xi(0)$ at each pressure (except at p = 40 torr) by assuming that, in each case, the experimental shortest-time datum lies on the free streaming region. This allows us to obtain $\alpha(t)$ at the remaining times. It is convenient to introduce an effective "mean free time," t_0, by the definition $D(\infty) \equiv \frac{1}{3}\langle v^2\rangle\ t_0$. For a low density gas, t_0 is inversely proportional to the pressure: $t_0 \equiv (mk_BT/6)^{1/2}/(p\sigma)$, where σ is an effective cross section of the Ca*-Ar scattering. An estimate of σ is obtained by assuming that $\alpha(t)$ is in the diffusion limit for the highest pressure (p = 40 torr) data and for p = 10 torr, t = 300 ns. The result is $\sigma = (20 \pm 14)\text{Å}^2$, which is consistent with calculations based on the Coulomb approximation.[6] (Note, however, a more precise determination is mentioned below.) The third and fourth columns of Table 3.I show the experimental times relative to t_0 and the reduced quantity $\alpha(t)/D(\infty)t_0$. Clearly, both short and long times have been studied relative to the mean free time, although only sparsely. Figure 3.2 shows the experimental values of $\alpha(t)/D(\infty)t_0$ as a function of t/t_0. Also shown is the result for a simple model of the velocity autocorrelation function with exponential decay (such a model is well-known to be a good approximation at low density[7]). The corresponding form for $\alpha(t)$ is then

$$\alpha(t) = \frac{1}{3}\langle v^2\rangle\ t_0^2\left[e^{-t/t_0} + (t/t_0) - 1\right] \quad . \tag{3.5}$$

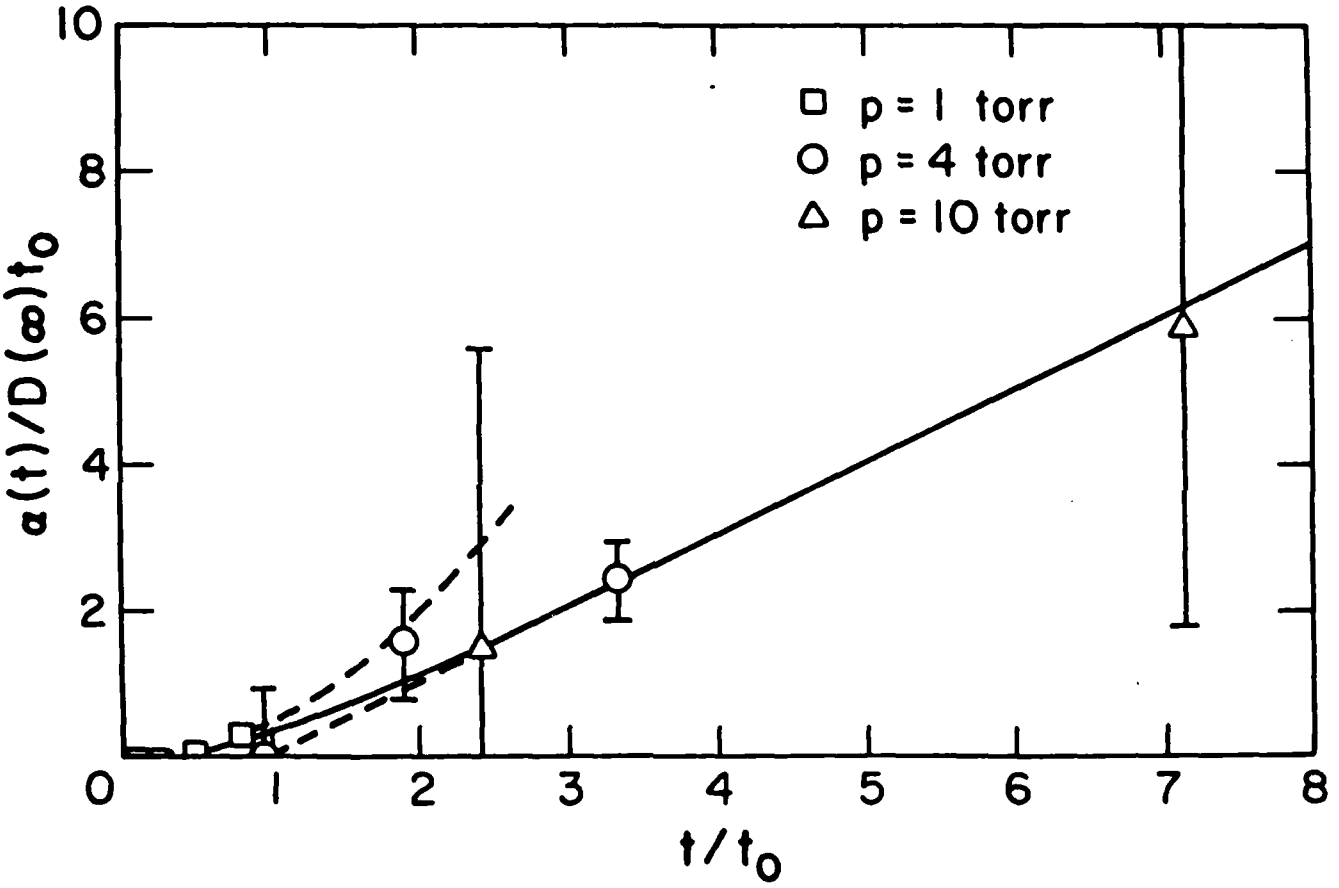

Figure 3.2 Plot of $\alpha(t)/D(\infty)t_0$ versus t/t_0 from the experimental data. The solid line corresponds to the model defined by Eq. (5). The asymptotic short time and long time behaviors are also shown (dashed lines).

This simple model is in reasonable agreement with the experimental points. A better fit could be obtained if one uses Eq. (5) to adjust $\xi(0)$ (at each pressure) and α. By doing so, the value $\sigma = (18.3 \pm 1.7)\ \text{Å}^2$ is obtained. We have also checked that the results are quite insensitive to the assumed shape of the pump and probe beams.

A repeat of this type of equilibrium experiment with higher precision is planned, to sample in detail the complete transition range, $0 > (t/t_0) < 100$. The measurements presented here were crude only because the time delays were limited by the electronics to about 350 ns. Experimental uncertainties could be considerably reduced by using longer time delays. One obvious advantage of this technique is the ability to determine diffusion coefficients of atoms and molecules in metastable states, for which conventional methods are inapplicable. Furthermore, the only other method for studying the transition region for tagged particles (inelastic neutron scattering) is limited to liquids or dense gases. The present method has the capacity to study this region at low densities where the theoretical developments are generally assumed to be most complete. In this sense it is an interesting complement to neutron and light scattering studies of fluids.

The experimental study of transport[8] and fluctuations[9] in nonequilibrium systems is even more limited. Nonequilibrium states involve changes in the hydrodynamic variables over space and time scales that are large compared to those sampled by light or neutron scattering. The deviations from equilibrium are measured by a uniformity parameter, $\mu = \ell/L$, where ℓ is the mean free path and L is the distance over which the relative changes in the hydrodynamic variables is of order 1. Current experimental methods are limited by a maximum value of ℓ (minimum density) because of signal loss. Consequently, to increase μ large gradients in the hydrodynamic variables must be produced;

convective instabilities and other problems have restricted the nonequilibrium states to $10^{-2} \lesssim \mu < 10^{-1}$. The method described here has the potential to improve on these limitations by increasing the mean free path, ℓ, instead of decreasing L. Since the fluorescence signals are easily detected at low pressures, μ can be increased simply by lowering the pressure. For example, at 10^{-1} torr the mean free path can be of the order of 10^{-1} cm. Thus the microscopic scales can be amplified to the macroscopic levels characterizing the nonequilibrium states available. For similar reasons the singular transitions from a collisional gas to a Knudsen gas can be studied for finite geometries, by changing the Knudsen number as a function of pressure. We are not aware of any alternative to spectroscopic techniques for investigation of such low densities. A class of nonequilibrium experiments along these lines is being explored.

4. An investigation into the effect of collisions on the ^3P_J manifold in Ca

Intersystem transitions fall in the class of lines which violate approximate selection rules. They violate the approximate electric dipole selection rule for LS coupling, $\Delta S = 0$. There is some confusion as to the effect of a collisional environment on oscillator strengths in the laboratory system comprised of a group IIA metastable ^3P state, as perturbed by rare gas atom collisions. Some authors claim to have observed collisional induced effects,[10] although others have not.[11,12,13]

In this section we describe our experiments on the $^1S_0 \rightarrow {}^3P_1^o$ spin-forbidden transition in Ca I, shown in Fig. 4.1. The estimated oscillator strength for this transition in the isolated radiator is 6×10^{-5}.[14] It is quite routine to produce ≈100 μJ of dye laser light in a single pulse using Nd:YAG technology, and so the number of excited states produced would be of

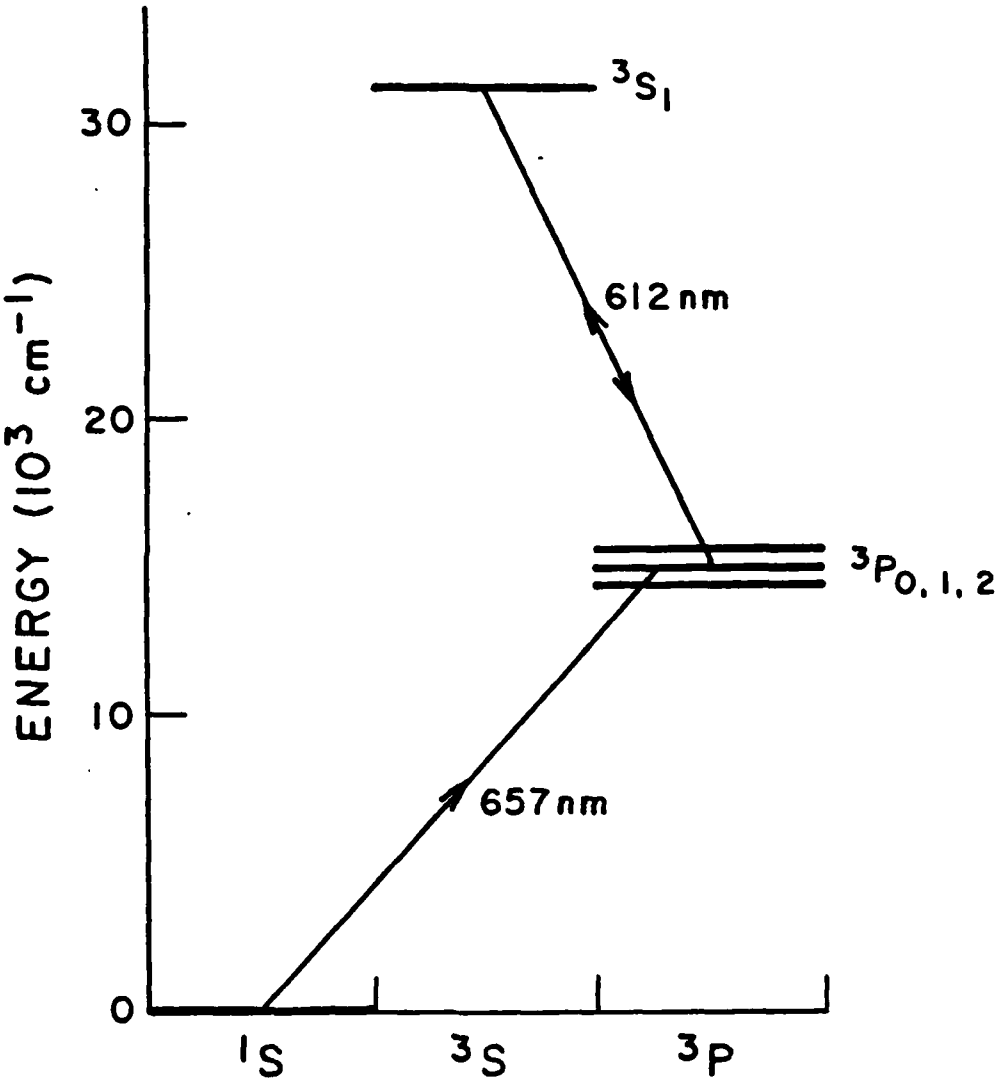

Figure 4.1

The spin-forbidden transition investigated in neutral calcium is shown together with observed emissions arising from energy pooling.

the order 10^{12}. Including a factor of 10^{-3} for the effect of photomultiplier cathode efficiency and light collection geometry based on a typical laser induced fluorescence (LIF) cell, we might expect to detect 10^{12} photons per second.

This detection rate is sufficiently fast that the effects of a collisional environment on the $^1S_0 \rightarrow {}^3P_1^o$ transition may be monitored most simply by observing the natural fluorescence of the $^3P_1^o$ state as a function of time. Collisional effects would manifest themselves as a non-zero quenching cross section, extractable from the observed effective fluorescence lifetime. A rate equation embodying these effects can be written

$$\frac{\partial}{\partial t}[Ca^*] = -\frac{[Ca^*]}{\tau} - k_q [Ar][Ca^*] = -\frac{[Ca^*]}{\tau_{eff}} \quad . \qquad (4.1)$$

In this equation $[Ca^*]$ denotes the concentration of excited Ca atoms formed after dye laser excitation, k_q is a quenching rate constant and [Ar] is the concentration of buffer gas particles, here taken to be argon. In fact, the lifetime due to spontaneous emission in the isolated atom, τ, is not the lifetime of the $^3P_1^o$ state itself, but rather a lifetime including the effects arising from the fact that the $^3P_1^o$ level is not isolated. It is a member of a $^3P_{0,1,2}$ fine structure multiplet. The decays of the $^3P_0$ and $^3P_2$ states are highly forbidden on the time-scale of the $^3P_1$ decay. Via fine-structure changing collisions[15] with the buffer gas, the ^3P_J multiplet is interconnected. The lifetime τ is therefore lengthened over the $^3P_1^o$ natural lifetime by a factor of roughly 2.8.[12] It will be noted that only quenching and decay have been included in Eq. (4.1).

In general, then, the experiments conducted involved the essentially instantaneous excitation of the ^3P_J manifold via a pulsed dye laser, and the observation of the effective fluorescence lifetime, τ_{eff}, as a function of

buffer gas pressure. The experimental apparatus is shown in schematic form in Fig. 4.2.

A doubled ND:YAG laser (Quanta Ray DCR2) excited a pulsed dye laser of the Shoshan design[16] operating on DCM dye (0.18 g/liter in methanol). The dye laser produced roughly 200 μJ ± 70 μJ of light near 657 nm. This simple design of dye laser operates on a few modes of individual line width controlled essentially by the number of grating lines subtended by an Amplified Spontaneous Emission (A.S.E.) spot on a grazing incidence holographic grating used as a wavelength selector. In these experiments, we used roughly 3 cm of a grating with 1800 lines per millimeter. However, jitter in the dye flow, mode competition, and other factors imply that the average line width of the laser (as measured by a scanning Fabry-Perot interferometer, for example) may be of order 5-10 GHz, or several times a doppler width. The output beam central spot is a superposition of many transverse modes and has a divergence that is essentially geometrically controlled, by cavity dimensions and pumped volume. The light at 657 nm was passed through a heated cell containing Ca vapor in an argon buffer gas. The cell was constructed of stainless steel, in a cross. The cell body was heated independently of a cold finger containing Ca metal. The cold finger controls the Ca vapor density if the finger temperature is below the cell body temperature. All such cells of a principally diffusion controlled design attain a quasi-steady Ca vapor density that is a balance between absorption and desorption on the calcium metal surface, and net diffusive losses to cold cell regions. For a cell consisting just of stainless steel tubes, the quasi-steady vapor density may be as much as a factor of 10 below the equilibrium vapor pressure. Moreover the diffusive rate, and hence the vapor density, are buffer gas pressure dependent. For the $^3P_1^o$ experiments an unaltered

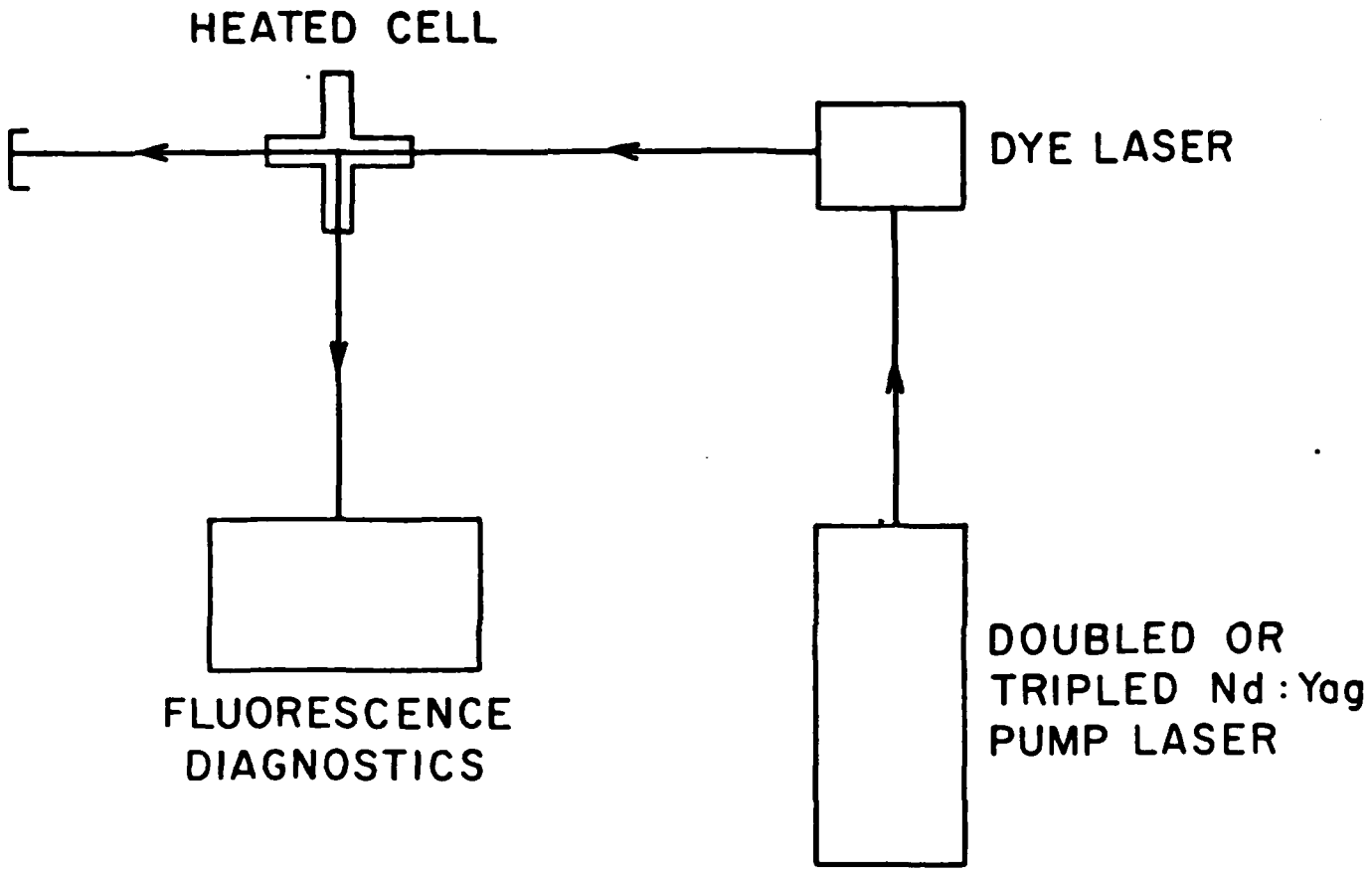

Figure 4.2 **A schematic of the spin-forbidden transition experimental apparatus.**

stainless steel cross was used, although gauze inserts in the cell arms prevented excessive plating of the cell windows and will have provided a certain "wick" action returning Ca to the center of the cell. (The wick action will not have been complete, since this cell is far from operating in a heat pipe mode.[17])

The fluorescent emissions from the Ca ^3P_J manifold were observed by a photomultiplier (EMI type 9789) in close proximity to the cell arm perpendicular to the path of the dye-laser beam, maximizing the available solid angle for detection. Wavelength selection was provided by an interference filter. The charge pulses emitted by the photomultiplier (PMT) were integrated by an RC circuit. The RC time construct was chosen at 1 μs which is long compared to the time duration of the charge pulses, but short compared to the ^3P_J isolated-atom lifetime. The integrated charge pulses were passed to a digitizing oscilloscope (Hewlett-Packard type HP54200) and averaged over 100 dye laser pulses. It is important to consider the oscilloscope offsets.

Logarithmic/linear plots of the observed decay permitted lifetime extraction. No deviation could be observed (to within 2%) from exponential decay. This was mainly the result of keeping the dye laser beam unfocussed. If tightly focussed, the dye laser would excite a "pencil" of Ca atoms, which would then diffuse away from the excitation volume, and possibly from the detection volume. By the time the dye laser beam passed through the cell, its transverse beam dimension was of the order of 5 mm, and at 300 τ of buffer gas, such an excitation volume could have spread by 14% in 1 ms.[18]

In such experiments involving decay over such long times (millisecond time scale) it is important to eliminate the effect of impurities. Such impurities as N_2 and H_2 (both very likely to be present, as a surface poison,

or end products of water gettering by hot Ca vapor respectively) have quenching rates far in excess of those expected for rare gas Ca^* quenching, and easily dominate results. It is important to bake out the cell in vacuum and after Ca loading at high buffer gas pressure, and to flush the system a number of times to reduce impurity concentrations. It is of course imperative to use high purity argon (99.9995% in our experiments). In our experiments two classes of impurities were seen. The first class was carried with the buffer gas, and could be gettered. The second class consisted of relatively chemically inert quenchers, that outgassed from the Ca metal and the cell.

Typical results from a set of experiments are shown in Fig. 4.3, taken with cell/finger temperatures of 650°C/600°C respectively. The inverse lifetime of the observed fluorescence decays is plotted against argon pressure. It will be noted that we judged our experiments to be effectively free from the effects of impurities when the extrapolation of our data to zero pressure (isolated calcium) lead to a lifetime in agreement (within errors) with the weighted average of previous lifetime measurements and calculations. The points on the right of Fig. 4.3 are taken from a table in Ref. 12, although severe outliers are ignored. The linearity of detection, and also saturation of the Ca vapor was checked using a variety of neutral density filters in the dye laser beam.

In our experiments we also noticed evidence of energy-pooling to the $^3S_1$ state shown in Fig. 4.1. The 610 nm emission observed had a lifetime of roughly 1/4 to 1/2 of that of the 657 nm emission. This emission is too slow to be associated with any process except $Ca^*(^3P_1)$ $Ca^*(^3P_1)$ collisions.

The above results immediately yield a new measurement of the isolated Ca atom lifetime (360 ± 20 μs), and also show that the cross section for quenching of Ca^* states is less than 5×10^{-23} cm^2, and, to within the errors

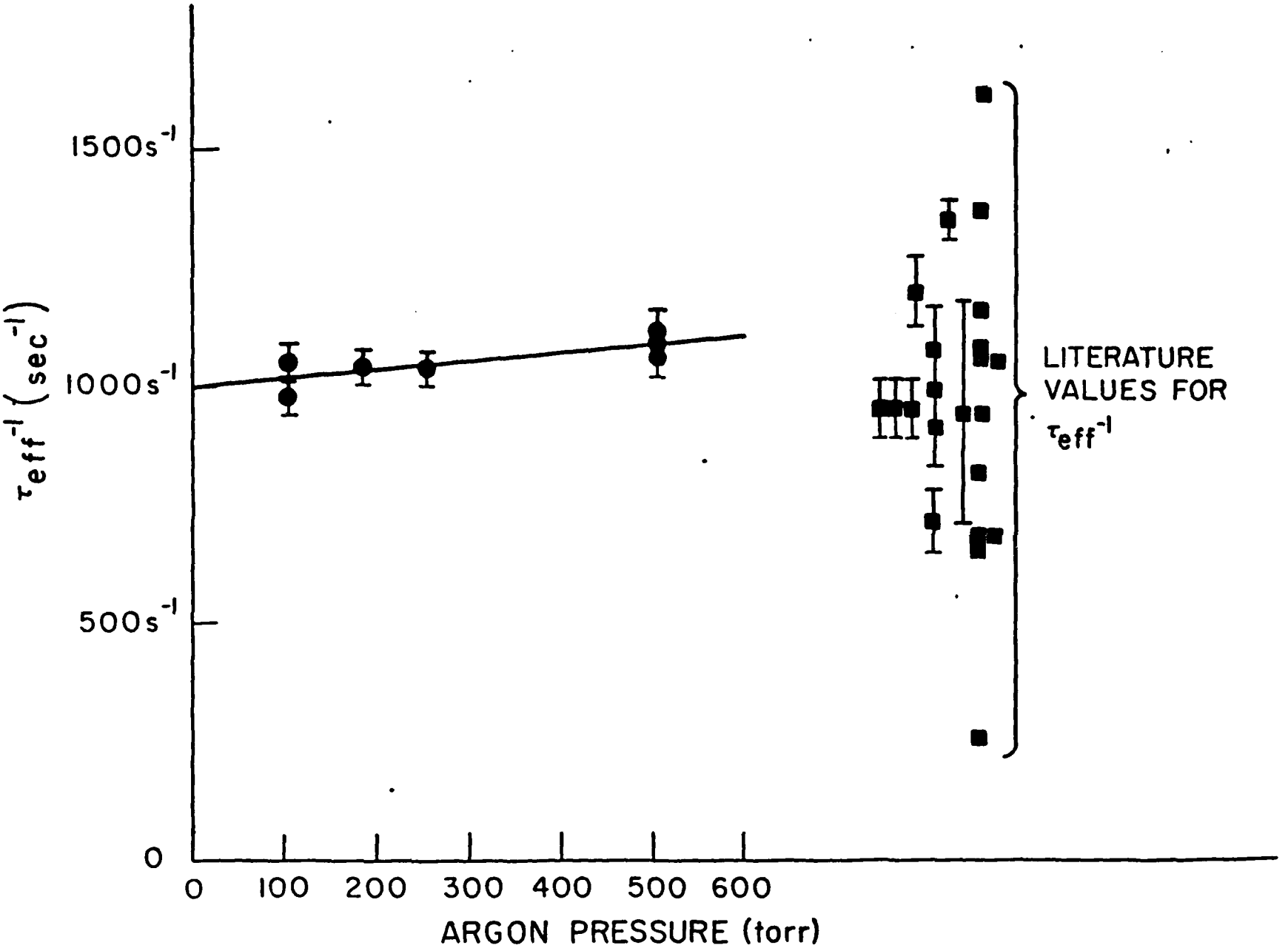

Figure 4.3

Results for the effect of argon pressure on the effective lifetime of the Ca $^3P_1$ level. Previous values for the isolated atom lifetime are shown on the right.

of this experiment consistent with zero. We may explain this essentially negligible result as follows. The intersystem transition probability is a result of the violation of the $\Delta S=0$ electric dipole transition rule appropriate for LS coupling. While in this paper, and elsewhere, LS coupling notation is used to describe the energy levels in Ca, it is quite clear that pure LS or jj coupling are idealizations never quite achieved in real atoms. Like all others, the Ca atom is an example of intermediate coupling -- a situation which arises whenever the $\underline{\ell}_i \cdot \underline{s}_i$ terms in the atomic Hamiltonian are not negligibly small in comparison to residual electrostatic terms. The net effect of intermediate coupling is to mix all states of the same J together. In an atom where LS coupling yields eigenstates between which the $\underline{\ell}_i \cdot \underline{s}_i$ interaction Hamiltonian has matrix elements small in comparison to the singlet/triplet splitting (arising from identical central field configurations) the net effect of intermediate coupling can be expressed perturbatively. The "$^3P_1$" state has various admixtures:

$$"|^3P_1\rangle" = |^3P_1\rangle + \alpha|^1P_1\rangle + \beta|^3S_1\rangle + \ldots. \qquad (4.2)$$

where α, β etc are $<<1$. An intersystem transition proceeds via these admixtures. Clearly the poorer the LS coupling approximation, the larger the admixtures and the higher the oscillator strength for intersystem transitions. This is indeed observed as a trend down a group of the periodic table, where the heavier the atom, the poorer the LS coupling approximation becomes.

Now, to first order, collisions between radiators and perturbers are described via an interaction Hamiltonian that is electrostatic in nature. Colliding partners, therefore, do not experience any increase of importance of $\underline{\ell}_i \cdot \underline{s}_i$ terms over electrostatic terms to first order, and so an intersystem transition should be, again to first order, unaffected by collisions. Clearly

this argument can be made more rigorous, but is expected to hold when the admixed states are detuned from the interesting states by significantly more than any possible Stark perturbations introduced via the transitory electric fields experienced by the radiator during the collision.

We are now in a position to discuss the quenching cross section results of others. Malins and Benard[10] have measured a cross section some three orders of magnitude larger than our result. We feel that their data may be subject to the effect of impurities (their argon was only 99.9% pure, or worse) in common with the conclusions of Husain and Schifino.[12,13] Furcinitti et al. have quoted an unpublished result for the cross section some three orders of magnitude lower than ours,[12,13] but bearing in mind the error bars published in Ref. 11, this seems somewhat optimistic.

In experimental conditions similar to ours, Granier et al. have also seen emission from $^3S_1$ at ~ 610 nm when pumping with a cw laser at 657 nm.[19] They attribute this to a possible formation of exciplex species. In our experiments, varying the calcium density, via varying the cell temperature, did not change the effective lifetime of the fluorescent emissions at 657 nm. Together with the time evolution of the 610 nm emissions, we feel that energy pooling is an altogether convincing explanation. The statement of Granier et al. that the 610 nm emissions are a two-photon effect is correct, since, clearly the two Ca^* atoms colliding to form $Ca(^3S_1) + Ca(^1S_0)$ are both the result of single photon absorption.

5. Modification of electronic exciation transfer collision cross sections with an ac Stark effect

There has been considerable interest recently in the properties of the metastable ^3P_J states in magnesium as a storage medium for proposed chemically

pumped visible lasers. The usefulness of such metastable levels depends on the ease of extraction of the stored energy. It is important to study possibilities of modifying electronic energy transfer collision cross sections. One possibility is outlined here: an energy transfer cross section can be manipulated by using an ac Stark effect. A schematic of a demonstration scheme is shown in Fig. 5.1. A strong laser tuned between excited states of strontium generates dressed states which may be placed into and out of resonance with the Mg $^3P_1$ state. The strong laser acts as a cross-section "switch." We present here a method of estimating the cross-section for energy transfer both when the switch laser is off, and when the dressed states are in resonance.

In order to present the physics of this scheme as clearly as possible, we simplify the problem. The Sr and Mg atoms interact collisionally via the dipole-dipole electrostatic interaction. We consider one binary collision in the absence of buffer gas. The strong laser is linearly polarized, of constant intensity and connects only the Sr and $^1P_1$ and $^1S_0$ states shown in Figure 5.1. We will consider there to be population only in the $m_J = 0$ level of Sr $^1P_1$ initially, and we estimate the cross-section for energy transfer for trajectories that are straight line classical paths.

The Schrödinger equation for the binary collision is written

$$i\hbar\frac{\partial}{\partial t}\left|\Psi\right\rangle = [H_{Sr} + H_{Mg} + H_E(t) + V(t)]\left|\Psi\right\rangle \qquad (5.1)$$

where the perturbations H_E and V are due to the strong field and the collision respectively. The effect of H_E is taken into account by creating "dressed states," the complete set of orthogonal eigenfunctions of $H_{Sr} + H_{Mg} + H_E(t)$. This set is then used to treat the collision in first order time dependent

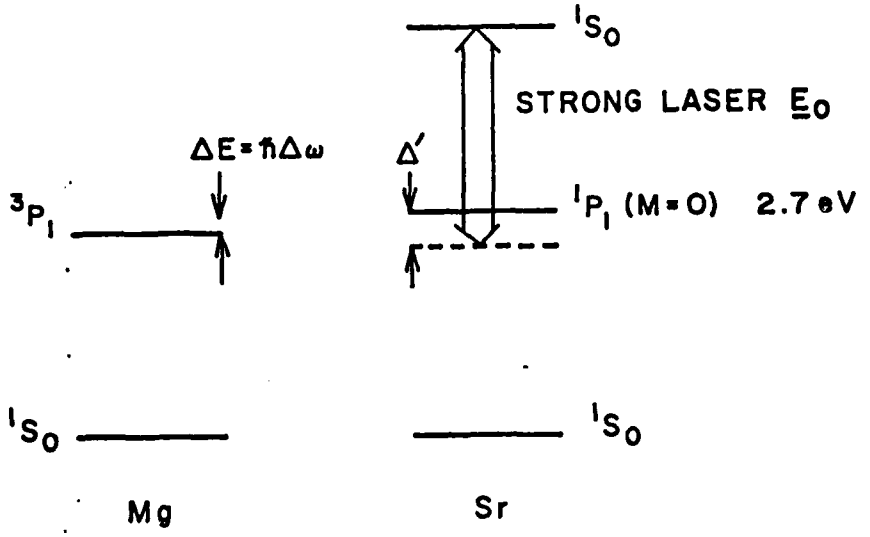

Figure 5.1 The proposed excitation transfer scheme.

perturbation theory. In this way we generate a set of equations for the eigenfunction amplitudes.

$$i\hbar\,\dot{a}_m = a_I V_m b_1 e^{i(b_2^2\Omega^1-\Delta\omega)t} + a_{II} V_m e^{i(b_1^2\Omega^1-\Delta\omega)t}$$

$$i\hbar\,\dot{a}_I = \sum_m a_m V_m b_1 e^{-i(b_2^2\Omega^1-\Delta\omega)t}$$

$$i\hbar\,\dot{a}_{II} = \sum_m a_m V_m b_2 e^{-i(b_1^2\Omega^1-\Delta\omega)t}$$

$$V_m = \langle Sr(J=1,M=0)\ Mg(j=0,M=0)\big|V\big|\ Sr(j=0,M=0)\ Mg(J=1,M=M)\rangle \qquad (5.2)$$

$$b_1 = [(\Omega^1+\Delta^1)/2\Omega^1]^{1/2}$$

$$b_2 = [(\Omega^1-\Delta^1)/2\Omega^1]^{1/2}$$

$$\Omega^1 = [\hbar^2\Delta^{12} + (\underline{E}_o \cdot \underline{d})^2]^{1/2}(1/\hbar)$$

In equations (5.2) we have assumed there are no curve crossings since we have ignored the non-resonant virtual excitations (via intermediate states other than those considered here) that contribute to Van der Waals type C_6 coefficients. In equations (5.2) a_m refers to the m-level of the target Mg state, and a_I and a_{II} to the two relevant states in the Sr atom. Also Δ^1 and $\Delta\omega$ are the mismatches between laser frequency and Sr $^1P_1$ - $^1S_0$ and the excitation frequencies of the P states respectively.

The strong field case is treated in the following manner - here $b_1 = b_2 = 1/\sqrt{2}$. By appropriate choice of Δ^1 and $\underline{E}_o$, i.e. $\Omega^1/2 = \Delta\omega$, it is possible to reduce equations (5.2) to a matrix equation reminiscent of resonance broadening

$$i\hbar \dot{a}_m = \frac{1}{\sqrt{2}} c V_m$$

$$i\hbar \dot{c} = \frac{1}{\sqrt{2}} \sum_m a_m V_m \qquad (5.3)$$

$$c = a_I + a_{II} \quad . \qquad (5.4)$$

Iterating on the initial condition $(c,a_m) = (1,0)$, and invoking a strong collision cutoff[20] we find a cross section (to within an order of magnitude)

$$\sigma = \frac{1}{\hbar v} (0.87) \quad \frac{h^2 e[gf_{Sr}\ gf_{Mg}]^{1/2}}{4\pi\epsilon_o mE} \qquad (5.5)$$

This is essentially a resonance broadening cross section.

In the low field limit, $b_1 = 1$ and $b_2 = 0$. In this case it is straightforward to show that no transfer occurs under an adiabatic approximation. Any transfer must occur via non-adiabatic effects. A method of calculating such processes (under the assumption that no molecular avoided crossings occur in the molecular potentials connecting assymptotically to the relevant Sr and Mg levels) can be derived by analogy to the work of Seaton.[23] A strong collision radius for the off-resonant case can be found in terms of one strong collision radius for the resonant case, discussed above.

Inserting numbers appropriate to the demonstration scheme shown in Figure 5.1, we find a low-field cross section of some 5Å^2 and a high-field cross-section of some 3000Å^2. Such enhancements have been observed under different conditions by Gallagher et al.[22] What we thus provide is proof-of-principle. The problem is in fact cylindrically symmetric, ideally requiring computer integration over trajectories[21]; moreover any experimental implementation of this scheme would require time dependent strong field laser intensities.

6. Theoretical investigations into collisionally induced absorption and emission

Collisionally induced transitions are transitions which are dipole forbidden, but which may be observed to have significant integrated-over-wavelength oscillator strength. Let us consider an excitation process such as

$$R(i) + P(g) + \hbar\omega \rightarrow R(f) + P(g)$$

in which a neutral atom or molecule (radiator R) undergoes collisions with neutral perturber atoms (perturbers P) under the influence of a radiator field of frequency ω. Since the $i \rightarrow f$ transition is electric dipole forbidden, this excitation process can procede via (a) a higher order multipole transition, e.g. electric quadrupole etc., or (b) a dipole moment induced by the collisional interaction.

The transition rate due to mechanism (a) is centered around the frequency of the dipole-forbidden transition $(E_f-E_i)/\hbar$ with a width determined by a typical impact collision rate γ_c. The transition rate due to mechanism (b) typically extends from $(E_f-E_i)/\hbar$ to detunings of a few times the inverse duration of a collision $(1/\tau_c)$ either to the red or to the blue. These collisionally induced transitions have been interpreted, in the main, as free-free dipole transitions between two molecular states of the radiator-perturber collision complex.[27] The lifetime of the transient collision complex, τ_c, determines the scale of the frequency dependence of the collisionally induced transition rate.

When experiments on collisionally induced processes are performed in a gas cell, the radiator density is usually far lower than the perturber density. If the perturber density is sufficiently low that strong collisions are well separated in time, (the binary collision regime), it is possible to

distinguish between single (intra-) collisional contributions and subsequent (inter-) collisional contributions to the observables of interest. The single collisional contribution is the standard molecular binary collision picture of the excitation process, but such a viewpoint masks possible interference effects which arise from correlations between the dipole moments induced during the first and subsequent collisions. The work of Lewis and Van Kranendonk[24] indicate that intercollisional effects lead to features in absorption spectra of width determined primarily by γ_c, in the case where lower state interaction is significant, for example vibrational or rotational transitions in molecular species. A common approximation made in atomic electronic transition line broadening studies (in contrast to molecular vibrational and rotational collisions) is that there is no interaction in the lower state. This is because electronically excited states are much more polarizable than ground states. The purpose of the work outlined in this section is thus twofold. First, a unified description of collisionally induced absorption is developed, valid in both impact and quasistatic regimes, and second, the ground work for a formalism is suggested which may be used to investigate the validity of, for example, the one-interacting-level (OIL) approximation, through the relative importance of the single, and subsequent collisional contributions to various observables. The formalism is based on master equations derived from equations describing the evolution of the density matrix describing the radiator-perturber system.

We consider one neutral radiator atom which collisionally interacts with N neutral noninteracting perturbers. The radiator and perturbers interact with an assumed classical monochromatic laser field

$$\underline{E}_c(\underline{x},t) = E_o \underline{\varepsilon}_\ell e^{-i(\omega t - \underline{k}_c \cdot \underline{x})} + \text{c.c.} \qquad (6.1)$$

and the transverse spontaneous modes of the radiation field represented by the electric field operator

$$\hat{\underline{E}}_s(\underline{x}) = \sum_{k,\lambda} [\hat{\underline{E}}_{k,\lambda}(\underline{x}) + \text{H.c.}] \tag{6.2}$$

with

$$\hat{\underline{E}}_{k,\lambda}(\underline{x}) = i\left[\frac{\hbar\omega_k}{2\varepsilon_o \bar{V}}\right]^{1/2} \underline{\varepsilon}'_{k,\lambda} e^{i\,\underline{k}\cdot\underline{x}} a_{k,\lambda} \tag{6.3}$$

and $|\underline{k}| = \omega_k/c$. The polarization of mode $(\underline{k},\lambda)$ is denoted by $\underline{\varepsilon}'_{k,\lambda}$ and $a_{k,\lambda}$ is the appropriate photon destruction operator. $\bar{V}$ is the quantization volume. The Hamiltonian determining the time evolution of this system is, for the radiative interaction in the dipole approximation, given by,

$$H = H_R + \sum_{j=1}^{N} \left[\frac{P_j^2}{2M} + H(j)\right] + \sum_{j=1}^{N} V(|\underline{x}_R - \underline{x}_j|)$$

$$- \sum_{j=R,1,..,N} \underline{\mu}_j \cdot \underline{E}_c(\underline{x}_j, t)$$

$$- \sum_{j=R,1,..,N} \underline{\mu}_j \cdot \underline{E}_s(\underline{x}_j) + H_F \tag{6.4}$$

with the free-field Hamiltonian

$$H_F = \sum_{k,\lambda} \hbar\omega_k a^+_{k,\lambda} a_{k,\lambda}. \tag{6.5}$$

In equation (6.4), H_R and H(j) are the Hamiltonians for the internal degrees of freedo of the radiator and perturbers, and $V(|\underline{x}_R - \underline{x}_j|)$ is the collisional interaction between them. The dipole moment of atoms j is denoted $\underline{\mu}_j$. Equation (6.4) explicitly ignores center of mass motion, thus we set $\underline{x}_R = 0$.

The density operator obeys the equation of motion

$$\frac{d}{dt}\rho_s(t) = \frac{1}{i\hbar}[H, \rho_s(t)], \quad t > 0 \tag{6.6}$$

In the interaction picture defined by

$$\rho_s(t) = U_o(t,0)\rho_I(t) \tag{6.7}$$

where

$$U_o(t,0) = \exp[L_R+L_F+\sum_{j=1}^{N}(Lp_j+L_j)]t \tag{6.8}$$

this reduces to

$$\frac{d}{dt}\rho_I(t) = [L_c^{(R)}(t)+L_S^{(R)}(t)+\sum_{j=1}^{N}[V_j(t)+L_c^{(j)}(t)+L_S^{(j)}(t)]]\rho_I(t) \tag{6.9}$$

in which Liouville operators are defined as

$$L_o O' = \frac{1}{i\hbar}[H_o, O'] \tag{6.10}$$

with

$$O'(t) = \bar{U}_o^{+}(t,0)O'\bar{U}(t,0) \tag{6.11}$$

and O' is an arbitrary Hilbert space operator. $\bar{U}_o$ is defined to be

$$\bar{U}_o(t,o) = \exp[\frac{1}{i\hbar}[H_R+H_F+\sum_{j=1}^{N}(H(j)+\frac{P_j^2}{2M})]t]. \tag{6.12}$$

We define a projection operator[25] in tetradic notation[25] by

$$P(\cdots) = |\{0\},\{0\}\rangle\rangle Tr_{RAD}[\prod_{j=1}^{N} p_j] \tag{6.13}$$

with

$$p_j = |g,g\rangle\rangle \rho(p_j) Tr_j(\cdots) \tag{6.14}$$

and RAD denotes spontaneous modes.

We denote the ground state of the perturbers by $|g\rangle$ and the density operator for the center of mass motion of the jth perturber by $\rho(p_j)$ (assumed to describe a normalized equilibrium situation.) The ground state of the spontaneous modes is denoted by $|\ 0\ \rangle$ and the trace over perturber variables by $\mathrm{Tr}_{\ p}$. Similarly Tr_j represents a trace over perturber degrees of freedom for the jth perturber and Tr_{RAD} a trace over spontaneous modes.

The reduced density operator of the radiator $\sigma_I(t)$ in the interaction picture is given by

$$\sigma_I(t) = \mathrm{Tr}_{RAD,\{p\}}\left(P\rho_I(t)\right). \tag{6.15}$$

The projected equation for the density operator which satisfies conditions for decorrelation at $t = 0$ ($Q = 1-P$, $Q\rho_I(t=0) = 0$) is the starting point for the calculation of observables like the collisionally induced excitation rate.

$$\begin{aligned}\frac{d}{dt} P\,\rho_I(t) = &\left[L_c^{(R)}(t) + P\sum_{j=1}^{N} V_j(t)P\right]\rho_I(t)\\ &+ P\left[L_s^{(R)}(t) + \sum_{j=1}^{N} V_j(t)\right]\\ &\times \int_0^t dt' G(t,t')\left[L_s^{(R)}(t') + \sum_{i=1}^{N}\left[Q\,V_i(t') + L_c^{(i)}(t') + L_s^{(i)}(t')\right]\right] P\rho_I(t')\end{aligned} \tag{6.16}$$

with

$$\frac{d}{dt}G(t,t') = \left[L_c^{(R)}(t) + QL_s^{(R)}(t) + \sum_{j=1}^{N}\left[L_c^{(j)}(t) + L_s^{(j)}(t) + QV_j(t)\right]\right]G(t,t')\ . \tag{6.17}$$

At this point approximations may be introduced into this equation of motion. The first is the binary collision approximation (BCA). The second is

the consideration of a well isolated $j = 0 \rightarrow j = 2$ transition with no consideration of higher order multipole transitions than electric dipole, no other atomic states in resonance and no contributing inelastic processes. The third approximation assumes that the Rabi frequencies induced by the laser are too small to affect the collision dynamics significantly, the fourth approximation is to assume the one interacting level approximation and the fifth approximation is to restrict the relevant detunings $|E_f - E_i - \hbar\omega_L| \ll kT_{gas}$.

We may perturbatively expand the propagator $G(t,t')$ in terms of $L_s^{(j)}$ and $L_c^{(j)}$. This expansion is inserted into equation (6.16). This allows us to write down an approximate equation of motion for the tensor multipole moments of the reduced density matrix for, for example, the excited state manifold of the radiator. This equation of motion is successively reduced to one perturber averages within the BCA. In this manner, master equations for the reduced density matrix of the radiator can be derived

$$\left[\frac{d}{dt} + \gamma + \frac{W}{2j_f+1}\right] \sigma_{ff}(t) = W\sigma_{ii}(t) \tag{6.18}$$

$$\left[\frac{d}{dt} + W\right] \sigma_{ii}(t) = \left[\gamma + \frac{W}{2j_f+1}\right] \sigma_{ff}(t) \tag{6.19}$$

to be solved with the initial condition $\sigma_{ii}(t=0) = 1$, $\sigma_{ff}(t=0) = 0$. The quantity W is the collisionally induced excitation rate and γ is the collisionally induced spontaneous decay rate. Equations (6.18) and (6.19) are single collision descriptions of the collisionally induced process, but in principle, corrections due to the subsequent collisional interactions as observed by Lewis and van Kranendonk may be included. W is shown to be

$$W = N \int d^3\underline{p}_1 \int \ldots \int d^3\underline{p}_4 \rho(\underline{p}_4) \times 2\,\mathrm{Re} \sum_{\alpha,\beta} \int_o^t dt' e^{i\omega t'} \frac{1}{\hbar^2}$$

$$\times \langle f\alpha g\underline{p}_1 | [D_c^{(R)}(t') + D_c^{(1)}(t')] | ig\underline{p}_2 \rangle^*$$
$$\times \langle f\alpha g\underline{p}_1, ig\underline{p}_2 | U_1^e(t',0) | f\beta g\underline{p}_3, ig\underline{p}_4 \rangle$$

$$\times \langle f\beta g\underline{p}_3 | [D_c^{(R)}(0) + D_c^{(1)}(0) | ig\underline{p}_4 \rangle$$

with the collisionally induced dipole coupling

$$\langle f\alpha g\underline{p} | D_c^{(j)}(t) | ig\underline{p}' \rangle$$

$$= \langle f\alpha g\underline{p} | [\underline{\mu}_j \cdot \underline{\varepsilon}\, E_o \frac{1}{H_R + H(1) - E_i - E_g} V(|\underline{x}_1|, t)$$

$$+ V(|\underline{x}_1|, t) \frac{1}{H_R + H(1) - E_f - E_g} \underline{\mu}_j \cdot \underline{\varepsilon}\, E_o] | ig\,\underline{p}' \rangle \quad j = R, 1 \tag{6.21}$$

Here V is the true collisional interaction, and we allow for the possibility that a dipole may be induced i either the radiator or the perturber.

Similarly,

$$\gamma = \sum_\lambda \int d^2k \frac{2\pi}{\hbar} \delta(E_f - E_i - \hbar\omega_k) \frac{\hbar\omega_k}{2\varepsilon_o (2\pi)^3} N \int d^3\underline{p}_1 d^3\underline{p}_2\, \rho(\underline{p}_2)$$

$$\times \frac{1}{2j_f + 1} \sum_\alpha |\langle ig\underline{p}_1 | [d_c^{(R)}(0) + d_c^{(1)}(0)] | f\alpha g\underline{p}_2 \rangle|^2$$

where

$$\langle ig\underline{p} | d_c^{(j)}(t) | f\alpha g\underline{p}' \rangle = \langle ig\underline{p} | [V(|\underline{x}_1|, 1, t) \frac{1}{H_R - H(1) - E_i - E_g} \underline{\mu}_j \cdot \underline{\varepsilon}'^*_{k,\lambda} \tag{6.22}$$

$$+ \underline{\mu}_j \cdot \underline{\varepsilon}'^*_{k,\lambda} \frac{1}{H_R - H(1) - E_f - E_g} V(|\underline{x}_1|, t)] | f\alpha g\underline{p}' \rangle \quad j = R, 1 \tag{6.23}$$

In equations (6.20) to (6.23) the label α is used to denote the magnetic sublevel of state $|f\rangle$. The details of the derivations may be found in the publication of Alber and Cooper,[44] who include an interesting discussion on the introduction of intercollisional coherences which may occur due to breadkown of spherical symmetry of the collisional environment due to motion of the atom through the ensemble. Such coherences may affect absorption in the vicinity of the forbidden line.

In the quasistatic region, W reduces to a form which can be obtained from the franck-Condon principle, i.e.

$$\begin{aligned} W &= \frac{2\pi}{\hbar}\frac{N}{V}\int d^3R_o \left|D(R_o)\right|^2 \delta\left(E_i + \hbar\omega_L - E_f - \Delta V_{fi}(R_o)\right) \\ &= \frac{2\pi}{\hbar}\frac{N}{V}\left|D(R_s)\right|^2 4\pi R_s^2 \left|\frac{d}{dR}\,4V_{fi}(R)\right|^{-1}_{R=R_s} \end{aligned} \tag{6.24}$$

with

$$\Delta V_{fi}(R_o) = \ll fg,ig\left|V_1^e(R_o)\right|fg,ig \gg \tag{6.25}$$

and

$$\begin{aligned} D(R) = \langle fg\Big|\Big[&(\mu_R+\mu_1)\underline{e}\,E_o \frac{1}{H_R - H(1) - E_i - E_g} V(R) \\ &+ V(R)\frac{1}{H_R + H(1) - E_f - E_g}(\mu_R+\mu_1)\underline{e}\,E_o\Big]\Big|\,ig\rangle \end{aligned} \tag{6.26}$$

and R_s determined from $E_i + \hbar\omega_L - E_f - \Delta V_{fi}(R_x) = 0$

Substantial work has also been undertaken on the expected spectrum of the photons emitted during the collisionally induced excitation process. In this case further approximations have been introduced - the first of which assumes that only the perturber dipole interacts with the spontaneous modes and the second is that during the generation of a spontaneous photon the influence of

all other spontaneous photons is ignored. These imply that

$\underline{\mu}_R = L_c^{(R)} = L_s^{(R)} = 0.$

The spontaneous emission rate is given by

$$\Gamma_{k,\lambda} = \frac{d}{dt} \ll 1,1 \left| \mathrm{Tr}_R \mathrm{Tr}_{\{p\}} \mathrm{Tr}_{RAD} [B \rho_I(t)] \right|. \tag{6.27}$$

in which

$$B = \prod_{j=1}^{N} p_J. \tag{6.28}$$

The quantity (6.24) can be formed and reduced via the BCA in analogous manner to the derivation of (6.20) and (6.22), with considerable algebra. Without going into details, the quantity Γ is comprised of three portions. The first is Rayleigh scattering, the second, absorption and emission during one collision and third, absorption during one collision and decay during another. The details may be found in the publication by Alber and Cooper.[44] Again, the extension to include the creation and destruction of coherences in two entirely separate collisions is made clear. Such coherences due to nonspherical symmetry caused by radiator motion could be anticipated to give rise to structure of the order of the width associated with the collisional broadening rate in the neighborhood of the forbidden line.

7. Experiments on the $Ca\ ^1D_2$ state - initial investigations

As stated previously, transitions of higher multipole moment than electric dipole, for example, electric quadrupole are termed forbidden transitions.[21] It is however possible to induce substantial oscillator

Figure 7.1

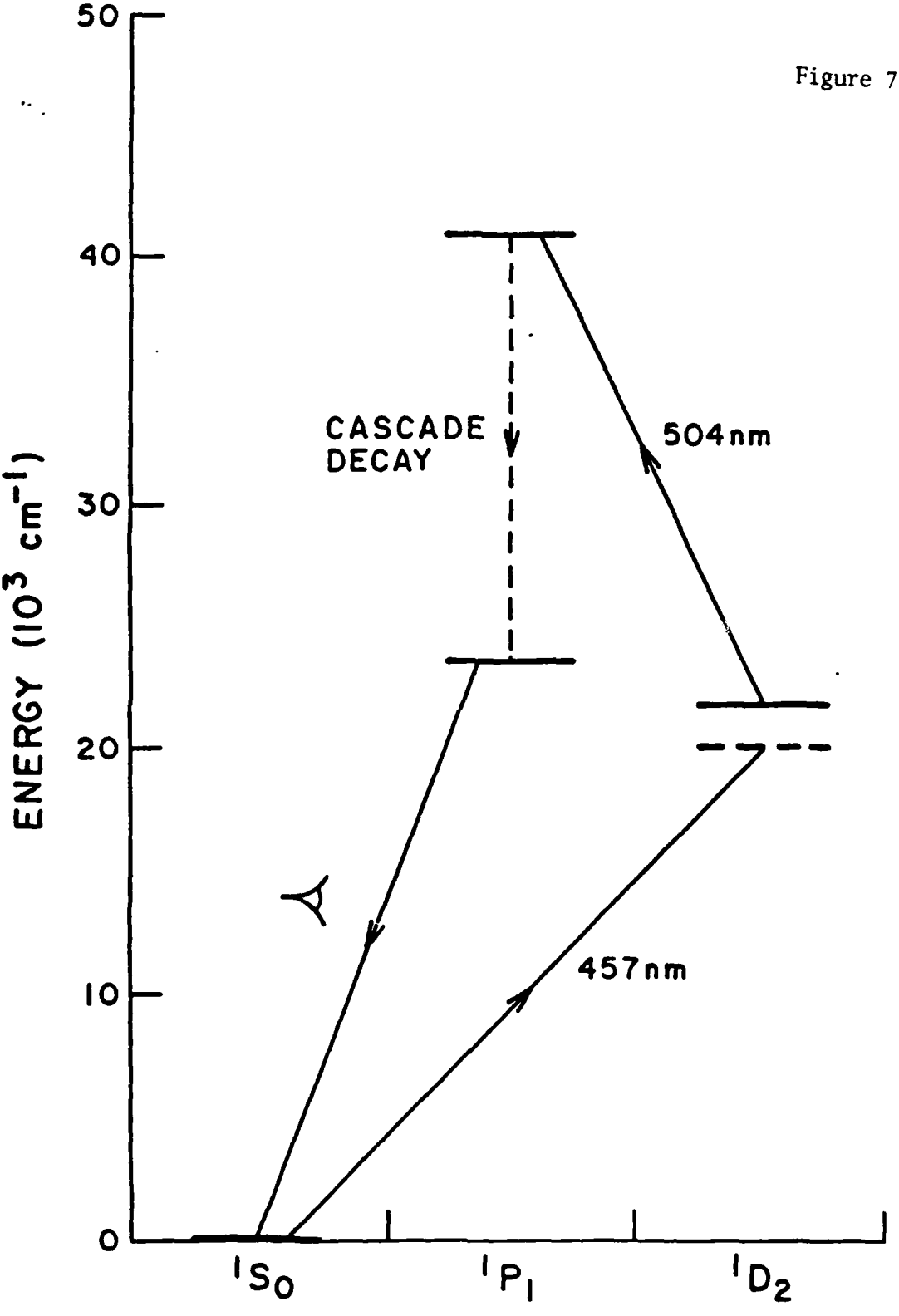

The electric quadrupole transition in neutral Ca is shown, together with the detection technique employed in the experiments

strength into a forbidden transition when the radiator (here denoted by R) undergoes collisions with perturbers (here denoted by P) in a process such as

$$R(|i\rangle) + P(|g\rangle) \rightarrow R(|f\rangle) + P(|g\rangle) \pm \hbar\omega,$$

in which i, f and g denote initial, final and ground states respectively. They have been qualitatively discussed for many years[27] and observed in a variety of radiator species.[28-38] Indeed collisionally induced effects have attracted attention from the laser design community, with regard to proposals for high power laser amplifiers.[39,40] These effects are also of interest to gas phase state-resolved chemistry. Several theoretical treatments of collisionally induced processes have proven convenient in interpreting observed effects,[41-43] and indeed the decomposition of the net effects into the various physical mechanisms responsible remains a topic of current interest.[44] All theories to date have treated spin-allowed transition only.

Now we turn our attention to the other transition of interest; the spin-allowed $^1S_0 \rightarrow {}^1D_2$ electric quadrupole transition in Ca I. This transition is shown in Fig. 7.1. Simple theory, e.g., Gallagher and Holstein,[43] can be used to estimate signal levels for this collision induced transition. For, say, Ca/Ar collision partners, the C_6 coefficients and other matrix elements of the electrostatic interaction required by the theory may be simply estimated using the Coulomb approximation and the radial matrix element of r^2 between $^1S_0$ and $^1D_2$ can be estimated from the results of Oertel and Shomo.[6] This estimate is only satisfactory to an order of magnitude since the Coulomb approximation can only be simply justified for Rydberg states. From these estimates we find that the absorption coefficient per unit bandwidth,

$$k_\omega d\omega \sim [Ar][Ca] \cdot 10^{-39} \text{ cm}^{-1} \quad . \qquad (7.1)$$

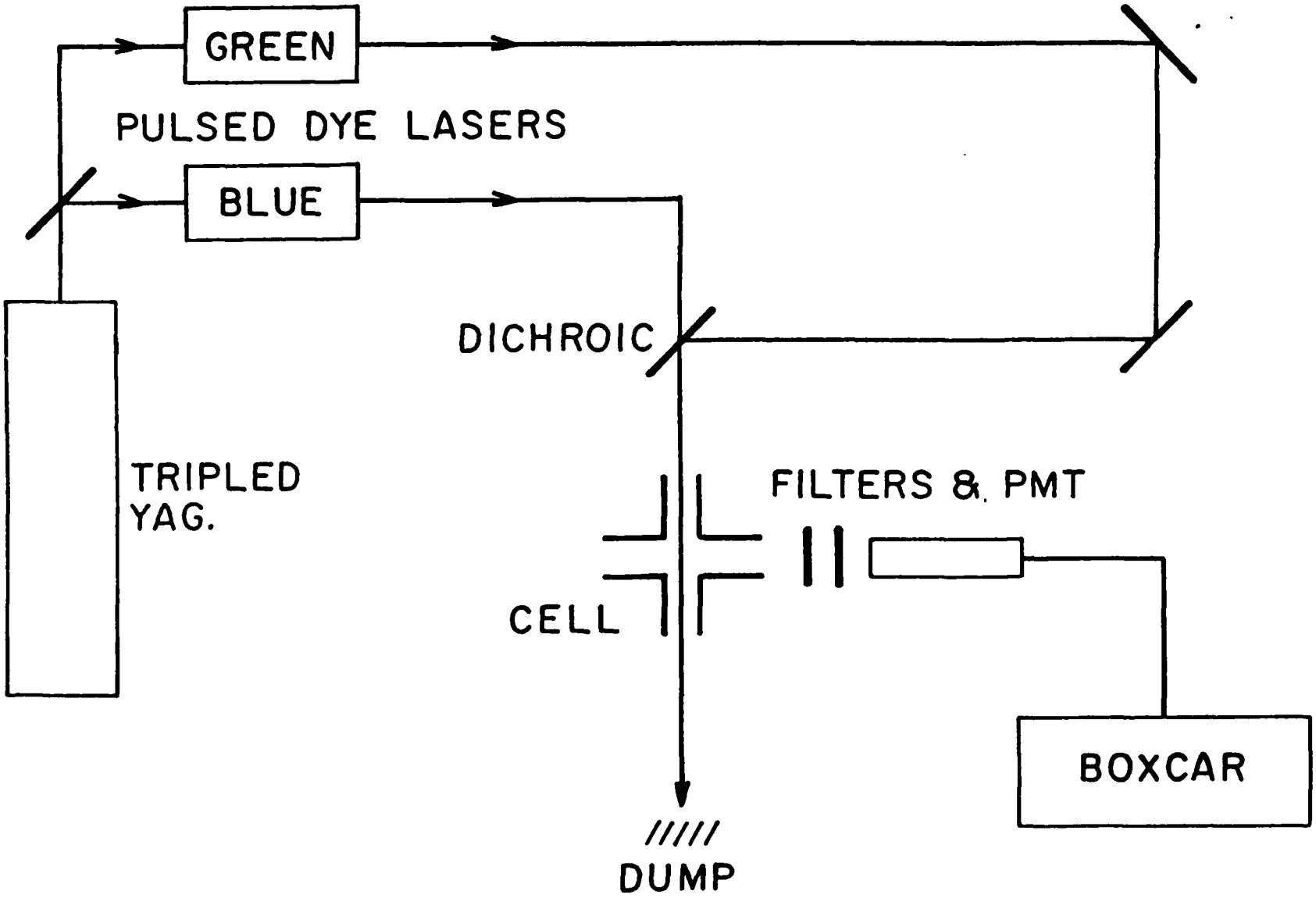

Figure 7.2 A schematic of the experimental apparatus used to investigate the electric quadrupole transition.

Even with a dye laser focussed into the cell, only 10^6 to 10^7 excited states in total are formed. Moreover, the decay of these states after the dye laser pulse has turned off occurs mainly by intersystem transitions with lifetimes of a few milliseconds. Indeed, during this time, the excitation pencil has expanded by a factor of at least 20. This implies that fluorescence from the pumped states would be extremely hard to detect experimentally. A probe-fluorescence detection technique was designed; the principal features are shown in Fig. 7.1. A second laser would probe the excited states, lifting them to a high-lying $^1P_1^o$ state. Since, in order to maximize the signal observed, we require high Ca densities (of at least 10^{15} cm^{-3}), optical decays of the high-lying $^1P_1^o$ state will be trapped to some extent. It is more convenient to observe the atoms that cascade down from the $^1P_1^o$ state via undetected photons to the resonance, lowest $^1P_1^o$ state — a bottleneck through which all cascading atoms must pass. Provided the calcium density is constant, a constant fraction of the excitations out of the $^1D_2$ state will be observed. This experimental technique requires the lifetime against collisional transfer from $^1D_2$ to other states to be long in comparison to the trapped lifetime of the $^1P_1^o$ states. It will be noted that collisional quenching cross sections are difficult to measure using this technique, but line shape data may be extracted by varying the frequency of the laser tuned to near 457 nm.

The experimental equipment used is shown in schematic form in Fig. 7.2 A tripled Nd:YAG laser (Quantel YG480) was used to pump two dye lasers, a "blue" one at about 457 nm (Coumarin 47, 0.15 g/liter in methanol) and a "green" one at 504 nm — the isolated atom $^1D_2 \rightarrow (4s6p)\ ^1P_1^o$ transition frequency (Coumarin 485 0.6 g/liter in ethanol). The beams were combined on a dichroic mirror, and roughly 30 μJ both blue and green beams, of 20 ns pulse duration, were

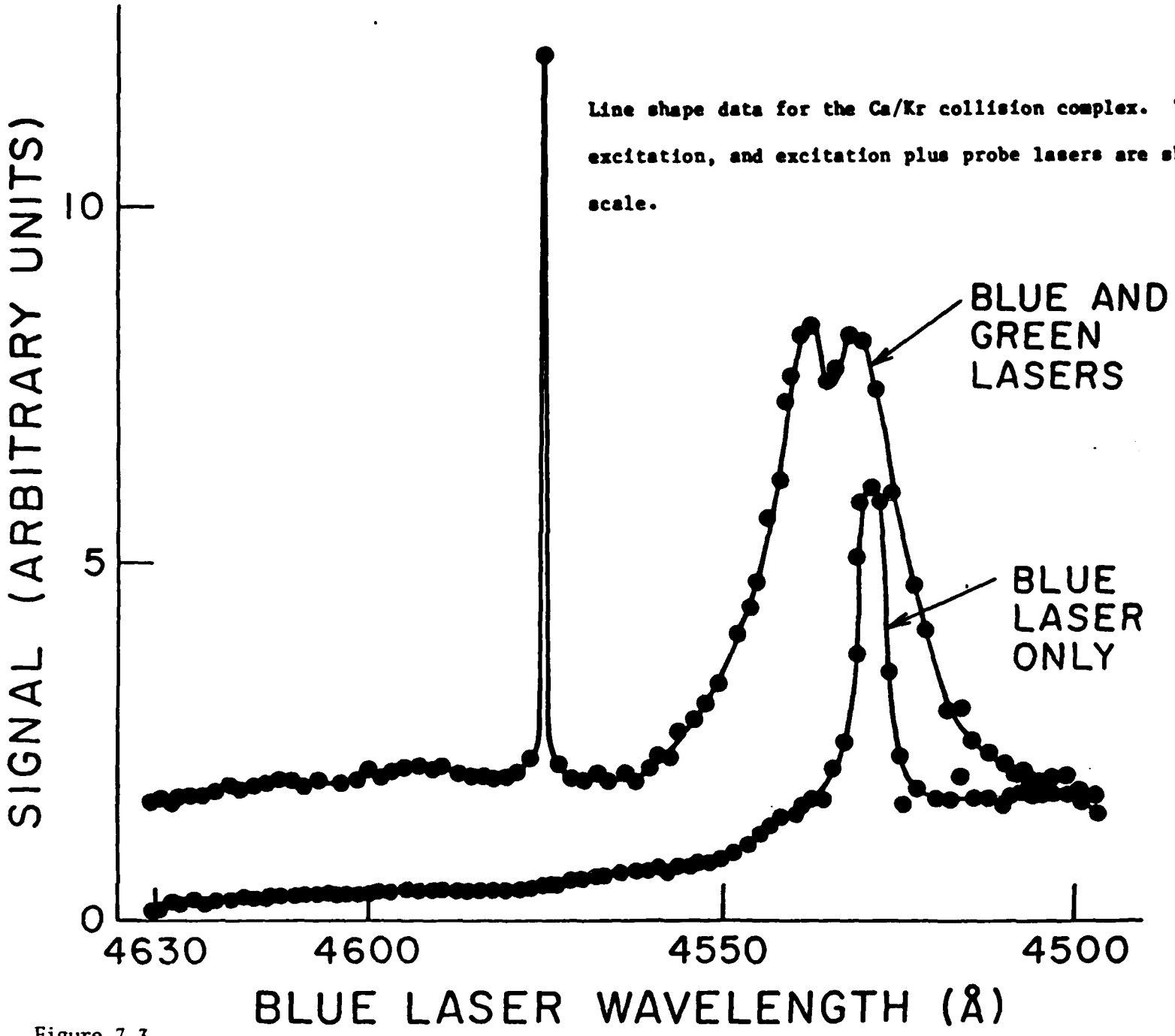

Line shape data for the Ca/Kr collision complex. The curves for excitation, and excitation plus probe lasers are shown on the same scale.

Figure 7.3

weakly focussed into the cell. In order to maximize the Ca density, baffles and gauze wicks were inserted into the hot cell zone down each cell arm. These structures reduced the solid angle for Ca diffusion away from the hot zone by a factor of 16. Measurements of the Ca density using the method of equivalent widths indicated that the equilibrium vapor pressure curves were being followed to within a factor of 2. The observable excitation pencil was roughly a cylinder of length 5 mm and diameter 1.2 mm. The fluorescence of the Ca resonance line was observed via an infrared blocking filter and a 420 nm Ca resonance line filter. The filter transmission full width half maximum of 10 nm intercepted essentially all the trapped, opacity-broadened Ca resonance light. Signals from a photomultiplier (EMI type 9829) were amplified and recorded via a boxcar amplifier (PAR type 160 series).

Thus, by tuning the "blue" laser and keeping the "green" laser fixed in frequency, line shape data could be extracted from the measured boxcar signal. It proved to be important to normalize out boxcar offsets and drifts, the frequency dependence of the transmission of the dichroic beam splitter, and drifts in the dye-laser output power. In this way, data on the $^1S_0 \rightarrow {}^1D_2$ transition were obtained for a variety of collision partners.

The collisional induced signal for the Ca/Kr collision complex is shown in Fig. 7.3 for cell/finger temperatures of 650°C/620°C respectively. Each point on these curves represents roughly 100 laser pulses. We have plotted two curves. The lower curve is the recorded boxcar signal for the excitation laser only, and the upper curve is the recorded signal for both excitation and probe lasers. The probe laser alone gives no observable signal. The errors on these data are typically ± 5% on each point. The E2 isolated atom transition is immediately seen at 4575 Å. More interesting is the blue laser signal around 4526 Å. This is the result of two sequential photons -- the

The collisional induced line shape data for the Ca/Ar collision complex. The curves for excitation, and excitation plus probe lasers are shown on the same scale.

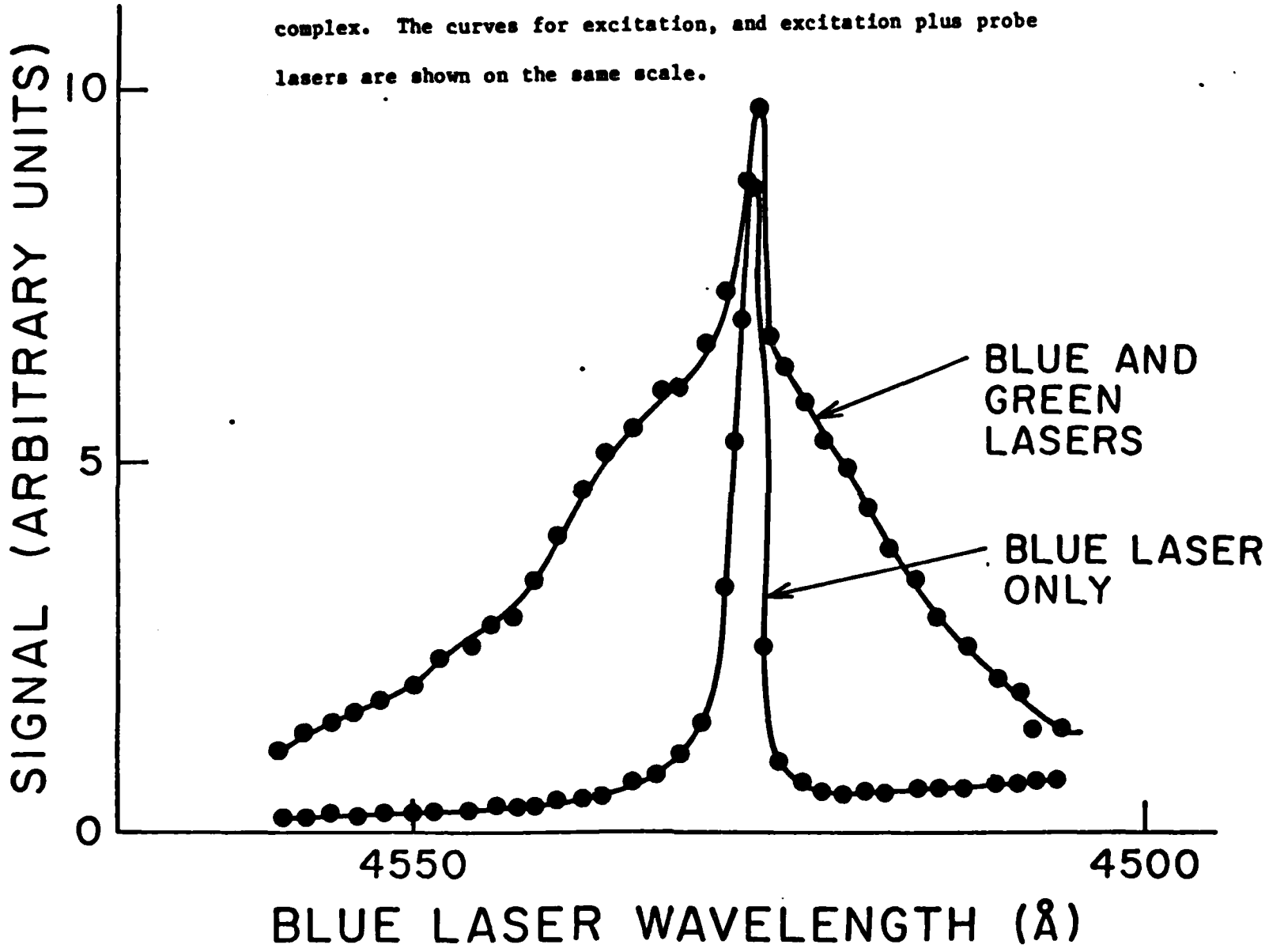

Figure 7.4

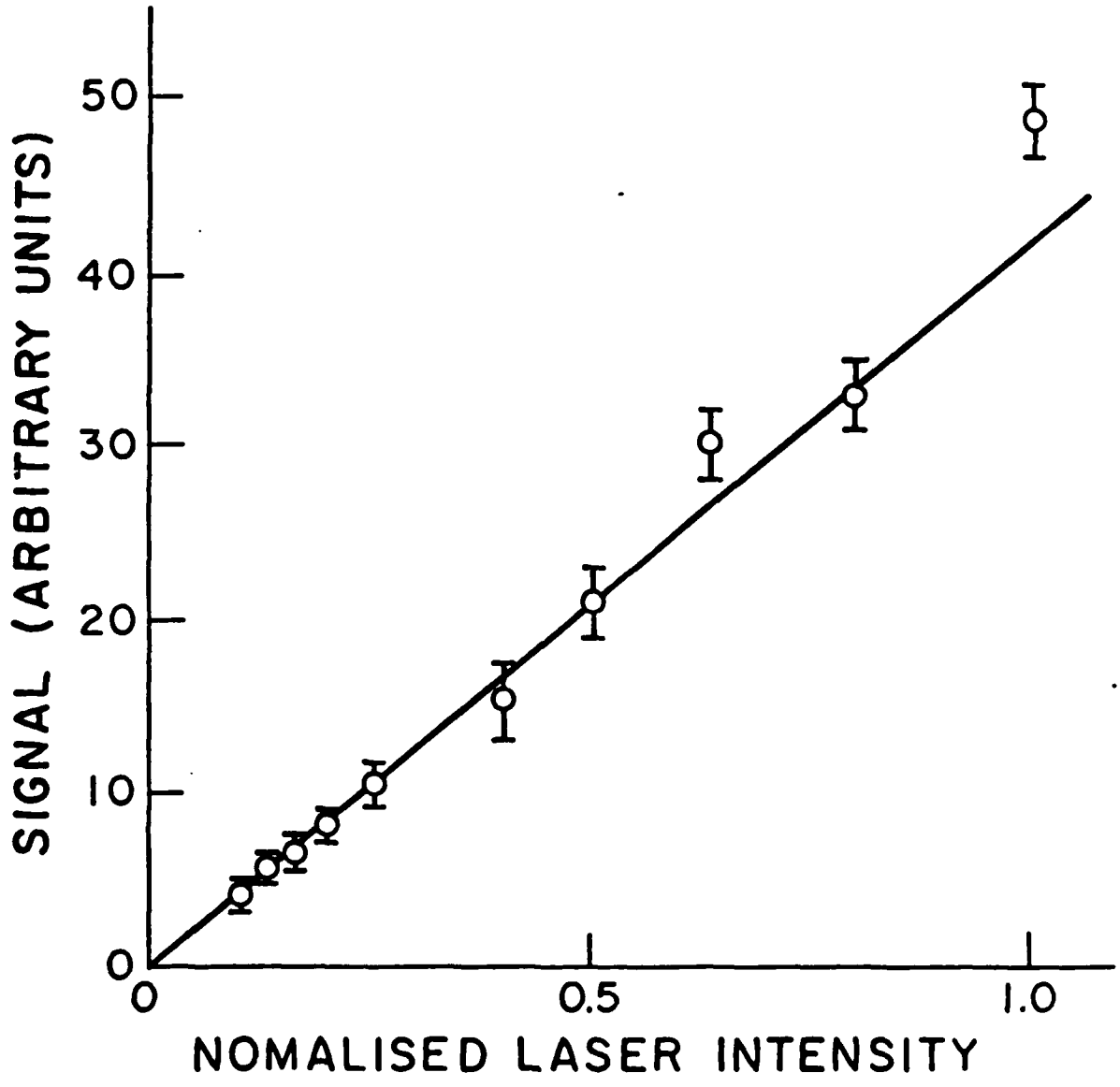

Figure 7.5

The collisional induced signal for the Ca/Ar collision complex as a function of excitation laser intensity, taken at an excitation laser wavelength of 4534 A.

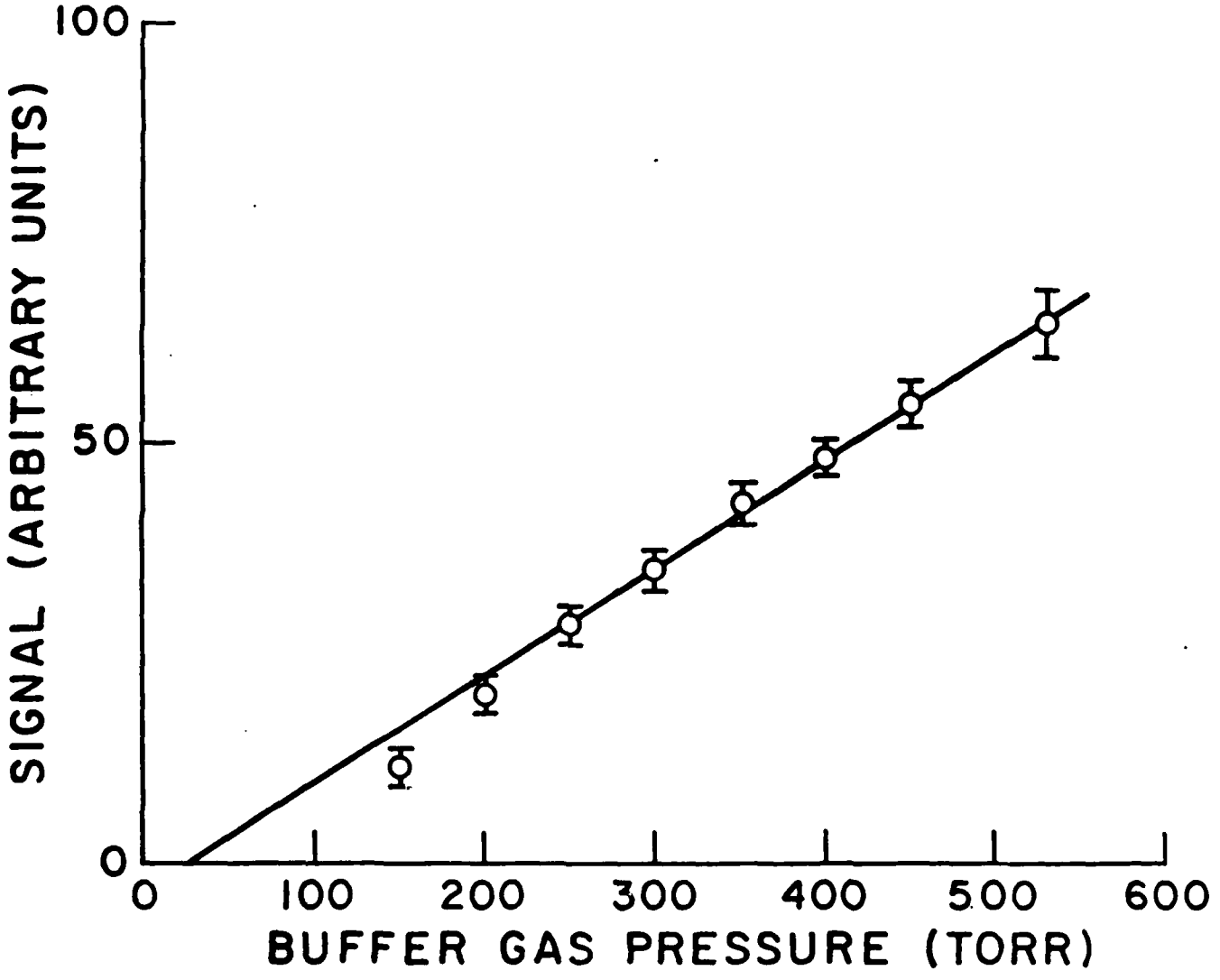

Figure 7.6

The collisional induced signal for the Ca/Ar collision complex as a function of buffer gas pressure, taken at an excitation laser wavelength of 4534 A.

first photon excites the collision complex, and the second excites the $^1D_2$ states to another high-lying $^1P_1^o$ state, from the 3d4p configuration, in a manner entirely analogous to the operation of the green 504 nm probe laser. It is the difference between these curves that is indicative of collisional induced excitation of the $^1D_2$ states.

We have also investigated the blue wing of the collisionally induced signal for the Ca/Ar collision complex. Those results are shown in Fig. 7.4. Unfortunately, the two sequential photon signal at 4526 Å falls on the peak of the collision induced signal, somewhat spoiling the quality of the data. There again, the error on each point is typically 5%. The cell/finger temperatures were 620°C/600°C respectively. Ca/Xe collision partners, however, yield ambiguous results. This is the result of a fast collisional process coupling the $^1D_2$ state to the triplet manifold ^3D_J in calcium. For these circumstances the diagnostic technique described in this report is not usable. The fast collisional process may be explained in terms of an unfavorable molecular curve crossing near the regions probed by the blue laser. This particular curve crossing has been invoked to explain surprisingly high $^1P_1^o \rightarrow {}^3P_1^o$ collisional relaxation rates observed in the Ca/Xe system by Wright and Balling,[45] and also by Harris et al.[46] All other Ca/rare gas collision partners are not subject to such unfavorable curve crossings.

Numerous two-photon processes are observed in these experiments, so it must be shown that the excitation of a $^1D_2$ state requires one collision and one blue laser photon. Figure 7.5 shows the collision induced signal observed as a function of blue laser intensity, for the Ca/Ar collision complex. The cell/finger temperatures were 620°C/600°C respectively. The data were taken with 4534 Å blue laser photons -- a region where the 4526 Å collision-aided

two-photon resonance contributed only minor error. The green 504 nm laser was left unaltered. The signal shows a linear dependence on blue laser intensity, indicative of a one photon process. Moreover, these results demonstrate the linearity of the detection scheme. Figure 7.6 shows the collisional induced signal as a function of buffer gas pressure, for the same conditions as Fig. 7.5. It will be noted that there is a slight roll-off at low buffer gas pressures. This may be attributed to increased diffusive loss of Ca, and possible increased plating of Ca metal on the cold cell windows. The data of Fig. 7.6 provide strong evidence that each Ca $^1D_2$ absorption requires one collision with a buffer gas atom for completion, at 4534 Å.

It is straightforward to show that spin-allowed electric quadrupole transitions may exhibit collisional induced effects.[43] We require that the electric dipole operator $\underline{d}$ connects the time dependent adiabatically modified states that asymptotically connect to the atomic produce basis states $|Ca\ ^1S_0,\ Ar\ ^1S_0\rangle$ and $|Ca\ ^1D_2,\ Ar\ ^1S_0\rangle$ (for the case of the Ca/Ar collision complex).

If the energy of interaction is small compared to the energy gap between the atomic states, then a perturbative $V/\Delta E$ expansion may be made, and the (time dependent through a collision) adiabatic states are then considered as linear combinations of atomic basis states. One such matrix element that appears in this approach is

$$\langle Ca\ ^1D_2\ Ar\ ^1S_0|V(t)\underline{d}|Ca\ ^1S_0\ Ar\ ^1S_0\rangle \quad , \tag{7.2}$$

in which V(t) is the collisional interaction.

Naively, one may consider the dipole operator to act upon the argon to produce a sum of intermediate virtual P states, such as to involve the following matrix elements:

$$\sum \langle Ca\ ^1D_2\ Ar\ ^1S_0 \,|V(t)|\, Ca\ ^1S_0\ Ar\ ^1P_1^o \rangle \langle Ca\ ^1S_0\ Ar\ ^1P_1 \,|\underline{d}|\, Ca\ ^1S_0\ Ar\ ^1S_0 \rangle \tag{7.3}$$

The electrostatic interaction V(t) may be written as a Coulomb expansion, and this expansion contains terms such as $V_{qd}^{(t)}$, the dipole-quadrupole interaction. $V_{qd}^{(t)}$ is precisely of the form to render the matrix elements in expression (7.3) non-zero, indicating that a collisional environment can indeed render collisionally perturbed electric quadrupole transitions connectable by a dipole operator. More sophisticated theory[44] gives essentially the same results if coherent contributions are ignored.

The above argument relies in part on a $V/\Delta E$ expansion. This approach is thus limited to regions where such an expansion is valid. Working within this region, Gallagher and Holstein[43] have developed expressions that may be used to predict line shapes if the collisional energy shifts of the atomic levels are described by C_6 coefficients. However, much of the physics may be extracted from simple quasi-static arguments, as in e.g. formula (6.23). If we consider the dipole operator $\underline{d}$ acting on the argon, as above, the matrix elements of V_{qd} vary like R^{-4} where R is the interatomic distance. Since the C_6-coefficient energy shift varies like R^{-6}, we expect the transition rate, W_P, to scale, in the quasi-static wing as[44]

$$W_P \propto \Delta\omega^{-1/6} \tag{7.4}$$

in which $\Delta\omega$ is the detuning from the isolated atom E2 transition.

If, however, we consider the dipole operator to act on the calcium radiator, it is the second order in V and higher matrix elements that contribute to the collisionally induced signal. Again assuming van der Waals

potentials for the relevant energy levels, we expect the transition rate in the quasi-static wing to scale at least as

$$W_R \propto \Delta\omega^{5/6} \quad . \tag{7.5}$$

This power law arises from the lowest possible contribution to the collisionally induced signal, as a result of a dipole-dipole and a dipole-quadrupole collisional interaction, and varies as R^{-7} instead of R^{-4}.

Consider now the ratio of W_R and W_P, the two possible contributions to a quasi-static spectral feature. It is straightforward to show that the ratio of intensities is (being the ratio of the matrix elements of the dipole operator considered to act in argon or in calcium taken between adiabatic states), assuming the transition occurs at the same interatomic radius,

$$\frac{W_R}{W_P} = \frac{|\langle\psi_{ad}^{out}|\underline{d}_{Ca}|\psi_{ad}^{in}\rangle|^2}{|\langle\psi_{ad}^{out}|\underline{d}_{Ar}|\psi_{ad}^{in}\rangle|^2}$$

$$\simeq \frac{|\langle {}^1S_0|\underline{d}_{Ca}|{}^1P_1\rangle|^2 \; |\langle {}^1P_1\,{}^1S_0|V_{dd}|{}^1S_0\,{}^1P_1\rangle|^2 \; |\langle {}^1S_0\,{}^1P_1|V_{dq}|{}^1D_2\,{}^1S_0\rangle|^2}{|\langle {}^1S_0|\underline{d}_{Ar}|{}^1P_1\rangle|^2 \; |\langle {}^1D_2\,{}^1S_0|V_{dq}|{}^1S_0\,{}^1P_1\rangle|^2 \; (E({}^1P_1)_{Ar} - E({}^1P_1)_{Ca})^2}$$

Note that we have included only the dominant contributions to the adiabatic states. Thus

$$\frac{W_R}{W_P} \simeq \frac{|\langle {}^1S_0|\underline{d}_{Ca}|{}^1P_1\rangle|^2 \; |\langle {}^1P_1\;{}^1S_0|V_{dd}|{}^1S_0\;{}^1P_1\rangle|^2}{|\langle {}^1S_0|\underline{d}_{Ar}|{}^1P_1\rangle|^2 \; [E({}^1P_1)_{Ar} - E({}^1P_1)_{Ca}]^2} \tag{7.6}$$

The convention $|Ca, Ar\rangle$ has been used in Eq. (7.6). It will be noted that the matrix elements of $\underline{d}$ are between resonance states, and may be estimated as the ratio of energies between the resonance states of calcium and

argon, since the f-values for the relevant transitions only differ by a factor of order unity.

$$\frac{W_R}{W_P} = \frac{E(^1P_1)_{Ar}}{E(^1P_1)_{Ca}} \frac{|\langle ^1P_1\ ^1S_0|V_{dd}|^1S_0\ ^1P_1\rangle|^2}{[E(^1P_1)_{Ar} - E(^1P_1)_{Ca}]^2} \tag{7.7}$$

From Eq. (7.7) it is clear that the increasing intensity with detuning component W_R cannot exceed the decreasing intensity with detuning component W_P without the $V/\Delta E$ expansion becoming invalid.

With the above information, we may interpret our line shape data. We do not see a spectrally decreasing with detuning component for one side of the E2 isolated atom transition. We do however see a large wing at detunings of the order of kT to the blue, and a weak wing again extending to the order of detunings roughly equal to kT. The fact that the blue wing increases from line center is convincing evidence that the observed oscillator strength in the collisionally induced signal for this transition comes from regions where the collisional interaction must be treated non-perturbatively, and the above simple power-law treatment breaks down. This is the region where precise molecular Born-Oppenheimer states provide the best description of energy levels. We are, of course, probing the transient molecules formed in calcium/rare gas collisions.

The only other data on this transition have been taken by Ueda and Fukuda[12] using a 60 cm, 1000°C absorption cell. While the 600°C laser induced fluorescence cell based experiments described here are technologically easier, our detection technique places restrictions on the collisional coupling rate between $^1D_2$ and ^3D_J states in calcium. Ueda and Fukuda have found evidence for a spectrally decreasing with detuning component close to the forbidden line for the Ca/Xe system, that is apparently describable within the framework

of a V/ΔE expansion. They have observed additional large blue wings, in common with our experiments, although these were left unexplained.

We may check that our data are consistent with those of Ueda and Fukuda, and the order of magnitude of the expected signal, since we were able to observe a two-photon excitation of a high-lying $^1D_2$ state in Ca, at 4658 Å. The peak of this two-photon signal is of the same order of magnitude as the peak of the large blue molecular wing observed in the Ca/Kr collision complex experiments. Using the standard expression for two-photon absorption,[47] and recognizing the fact that the laser linewidth is roughly five times the experimental doppler width, we may estimate the net effective absorption coefficient corresponding to the observed two photon signal. We may then compare the absorption coefficient to that seen experimentally by Ueda and Fukuda[37] for the blue wing in the Ca/Kr system. We obtain an absorption coefficient for the Ca/Kr blue wing as

$$k_\omega \cdot d\omega = [Kr]\ [Ca]\ (10^{-38}) \quad , \tag{7.8}$$

in order-of-magnitude agreement with Ueda and Fukuda.[37] It should be pointed out that this internal calibration procedure requires the replacement of the laser beam by a uniform cylinder of photons, of step function time evolution. Agreement to within an order of magnitude between the absorption technique and the two-photon technique is considered good, particularly since not all the excitation to the high-lying states via the green laser may cascade through the $^1P_1^o$ resonance state.

We also note that the collisional coupling between ^3D_J and $^1D_2$ in calcium may explain the high rate of collisional quenching of Ca ^3P_J by xenon observed by Husain and Schifino,[12] by invoking the inverse process to that discussed by Wright and Balling.[45] Moreover, the width of the blue two sequential photon

signal at 4526 Å indicates that potential information may be obtained for the excited state $^1D_2$ to high-lying $^1P_1$ transition.

8. Further investigations into the collisional induced transition in calcium

In this section the results of Sec. 7 are continued further to include Ca/He, Ca/Ne and Ca/Xe collision partners. This extension was made possible by rebuilding the detection electronics scheme.

For the experiments reported here, the broadband amplifier and boxcar used in Sec. 7 were replaced. A preamplifier (EGG ORTEC type 9301) was used to drive a heavily shielded cable to the rest of the data collection electronics. The reduced impedance of the cable earth return results in enhanced noise immunity. The incoming signal was further amplified using a timing filter amplifier (EGG ORTEC type 474). For constant cell temperature, the degree of Ca resonance light trapping is constant. Our signals then are pulses of uniform time evolution but variable amplitude. The amplitude of the signal contains information about the probability of exciting the Ca/Rare gas collision complex. Therefore, the timing filter amplifier may be used to enhance the signal-to-noise of the incoming photomultiplier pulses, by integrating over signals fast incomparison to the Ca resonance line light pulse evolution, and by differentiating out signals slow in comparison to the Ca light. Experimentally, for cell temperatures of the order of 650°C, the trapped Ca light evolves over a timescale of roughly 100 ns, and thus our amplifier was set to integrate with a time constant of 20 ns and differentiate over a timescale of 200 ns. While all such "artificial" signal processing techniques modify the noise statistics from gaussian (i.e. "white" noise becomes "colored") successive signal averaging reinstates gaussian statistics to an extent, via the central limit theorem. Residual discrepancies in the

The calcium/helium collisionally induced lineshape data. The curves for excitation and excitation plus probe lasers are shown on the same scale.

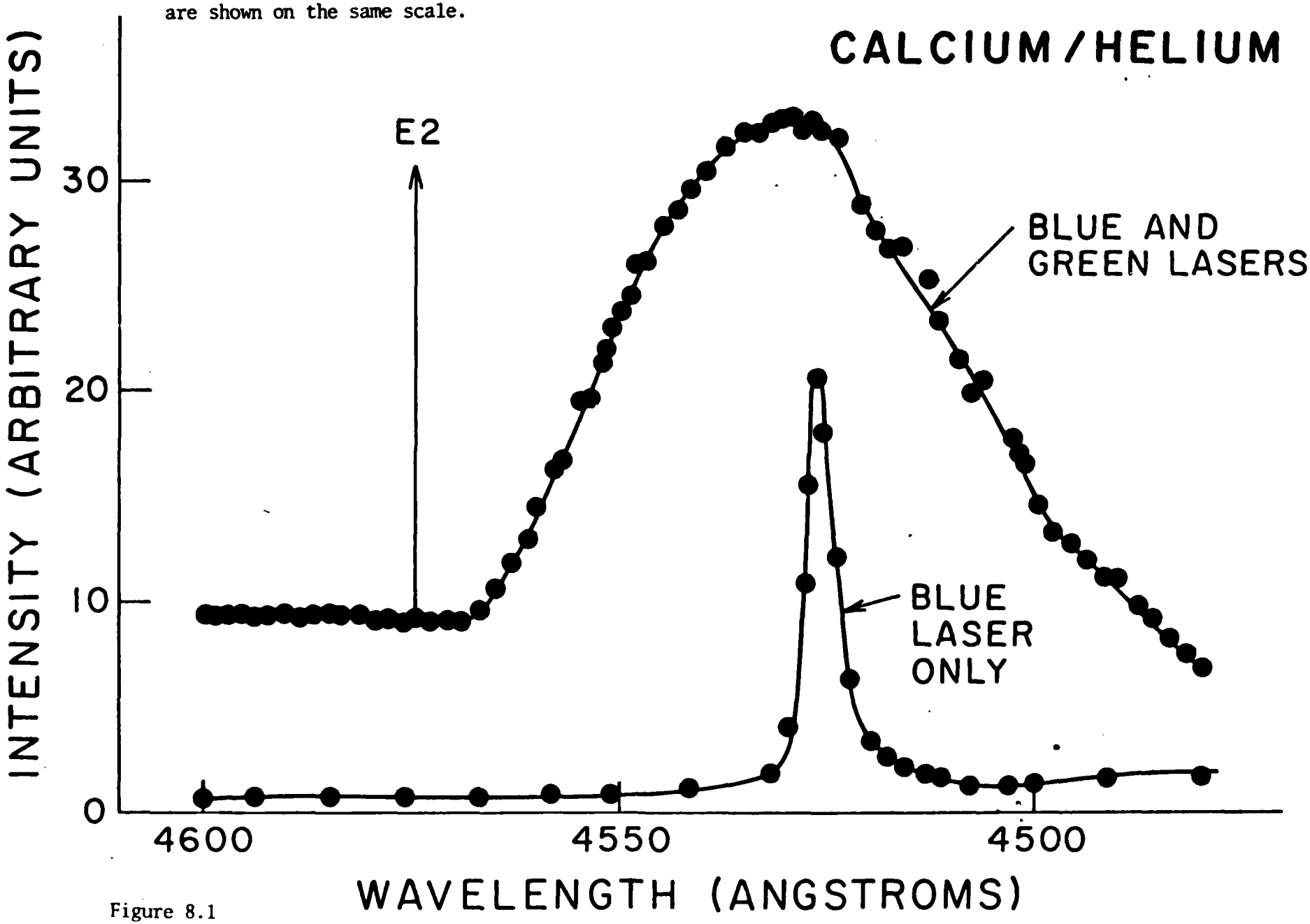

Figure 8.1

Figure 8.2 The calcium/neon collisionally induced lineshape data. The curves for excitation and excitation plus probe lasers are shown on the same scale.

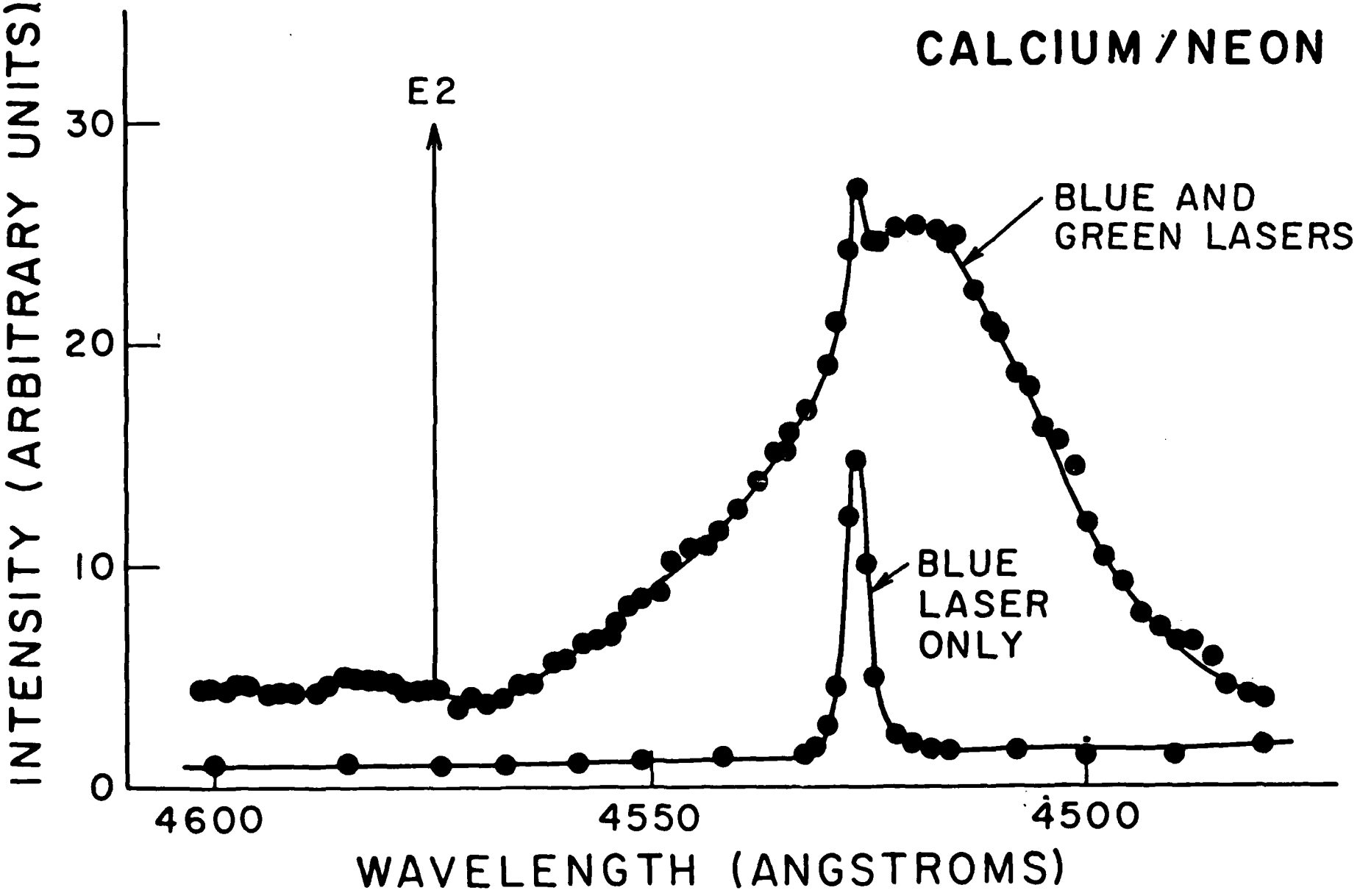

statistics from the idealized gaussian were ignored. The amplified pulses were then passed to a boxcar gated integrator (SRS type 250). The boxcar trigger was derived from the photodetection of dye laser light "upstream" of the cell. For some results it was appropriate to measure the boxcar running average signals with a digital voltmeter, it later proved essential to measure the signal from each boxcar event and process the results at a laser date via a computer interface (SRS type 245) and IBM compatible microcomputer (Wisetek type XT) running SRS 265 data aquisition software. As a final experimental point, the provision of variable amplifier gain allowed optimum combinations of gain and photomultiplier tube high voltage (hence signal and dark current) to be set for the different experiments consistent with detection linearity.

The above apparatus was used to investigate the absorption spectrum of the collisionally induced Ca $^1D_2$ transition for the collision partners Ca/He and Ca/Ne, taken for cell/cold finger temperatures of 625°/650°C and for buffer gas pressures of 500τ.

For both lineshapes it proved important to consider boxcar offsets and drifts, dye laser light intensity as a function of wavelength, and signal intensity drift as a function of time. The spectra obtained are shown in figures 8.1 and 8.2. Each point is subject to some 2% error and is the average of some 100 laser pulses. In both cases a broad background signal due to the blue ≈4575 Å laser was observed. This is the result of far wing collisional redistribution into the Ca $^1P_1^o$ resonance level. A feature close to 4530 Å in the blue laser signal is the result of absorption into the Ca $^1D_2$ state via the collisionally induced process followed by excitation to a high lying $^1P_1^o$ state in the free Ca atom - a member of the 3d4p configuration. This two sequential photon signal is the result of a process entirely analogous to the signal derived from the action of the green 504 nm laser.

The green laser by itself contributes negligibly to the observed signals, but in combination with the blue laser probes the collisionally induced absorption. The "blue laser only" and the "blue plus green" laser signals are plotted on the same scale. It is thus the difference between the signals that is indicative of collisionally induced absorption. In both cases a large blue wing and a weak red wing are observed on either side of the Ca $^1D_2$ 4575 Å E2 transition. These wings extend to detunings of the order of $kT/\hbar$ and are taken to be the result of oscillator strength found in the transient Ca/rare gas molecule. These signals are consistent with the oscillator strengths measured in the absorption cell experiment by Ueda dn Fukuda[27] although comparison of the vertical scales of our plots is difficult due to the uncertainty in the heated cell Ca density in our experiments. As such, our experimental signals are the result of the detection of the order of 1000 photoelectrons from the photomultiplier cathode.

It has been postulated that there is a molecular curve crossing between the moleculer potential curves asociated with Ca($^1D_2$)/Xe and Ca(^3D_J)/Xe. This would explain the unusually large Ca($^1P_1$) → Ca(^3P_J) relaxation rate observed by Wright and Balling, for Xenon as opposed to the other rare gases. This molecular avoided curve crossing contributes to an unobserved loss mechanism for collisionally induced Ca($^1D_2$) states in our experiment. Thus we find that our experimental procedure yields ambiguous results for the typical conditions of 625°C/650°C cell/finger temperatures and 500τ of buffer gas. However, changing the probe laser wavelength to a ^3D_J - $^3F_{J'}$ resonance allows poor quality data to be obtained from the Ca/Xe collision complex. The poor quality is the result of the degree of complication in the detection route - the $^1D_2$ states are formed, they become ^3D_J states, are lifted to $^3F_{J'}$, once more cross into the singlet system and then cascade to the resonance level.

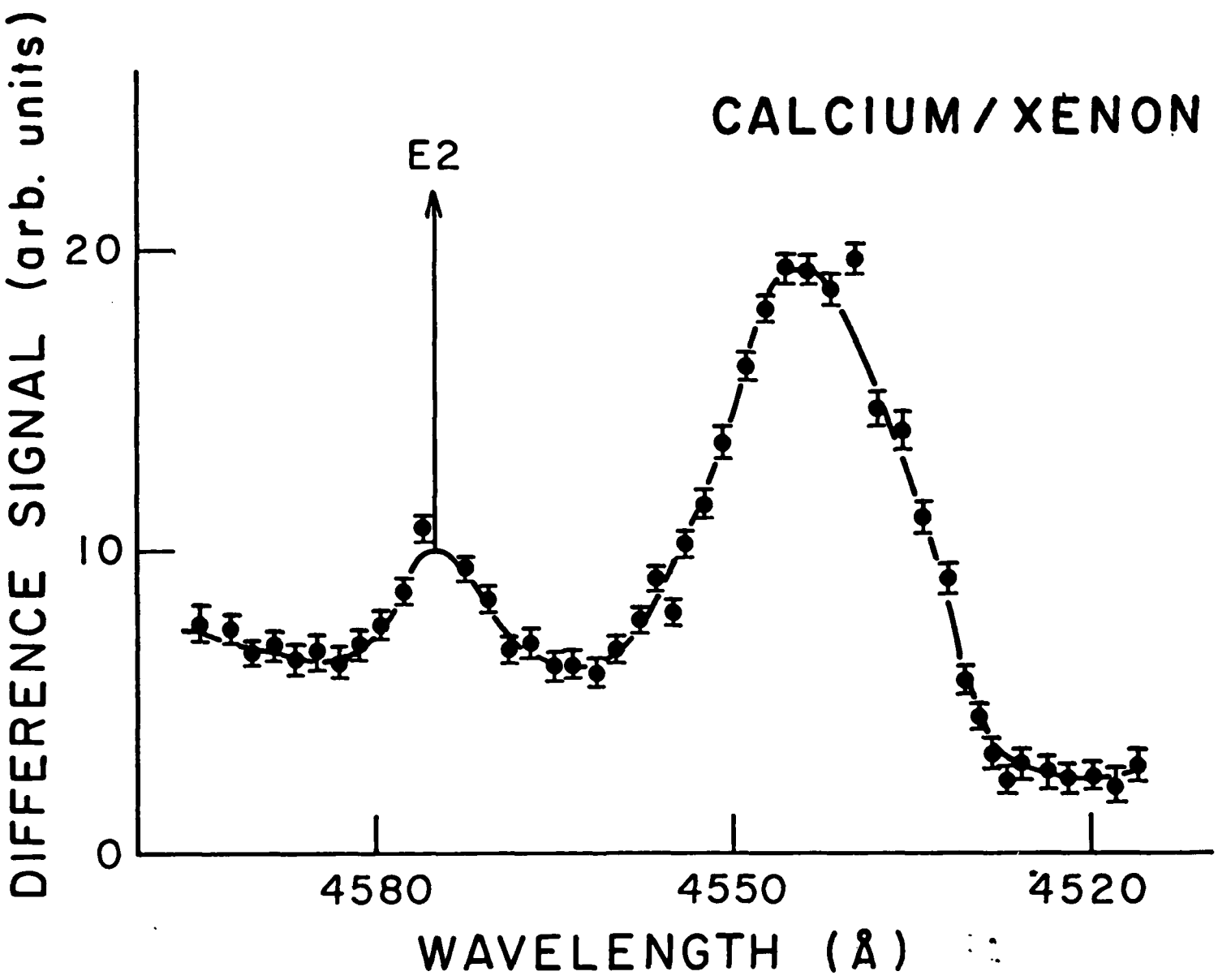

Figure 8.3 The calcium/xenon collisionally induced lineshape data. The difference signal between pump and pump plus probe signals is plotted.

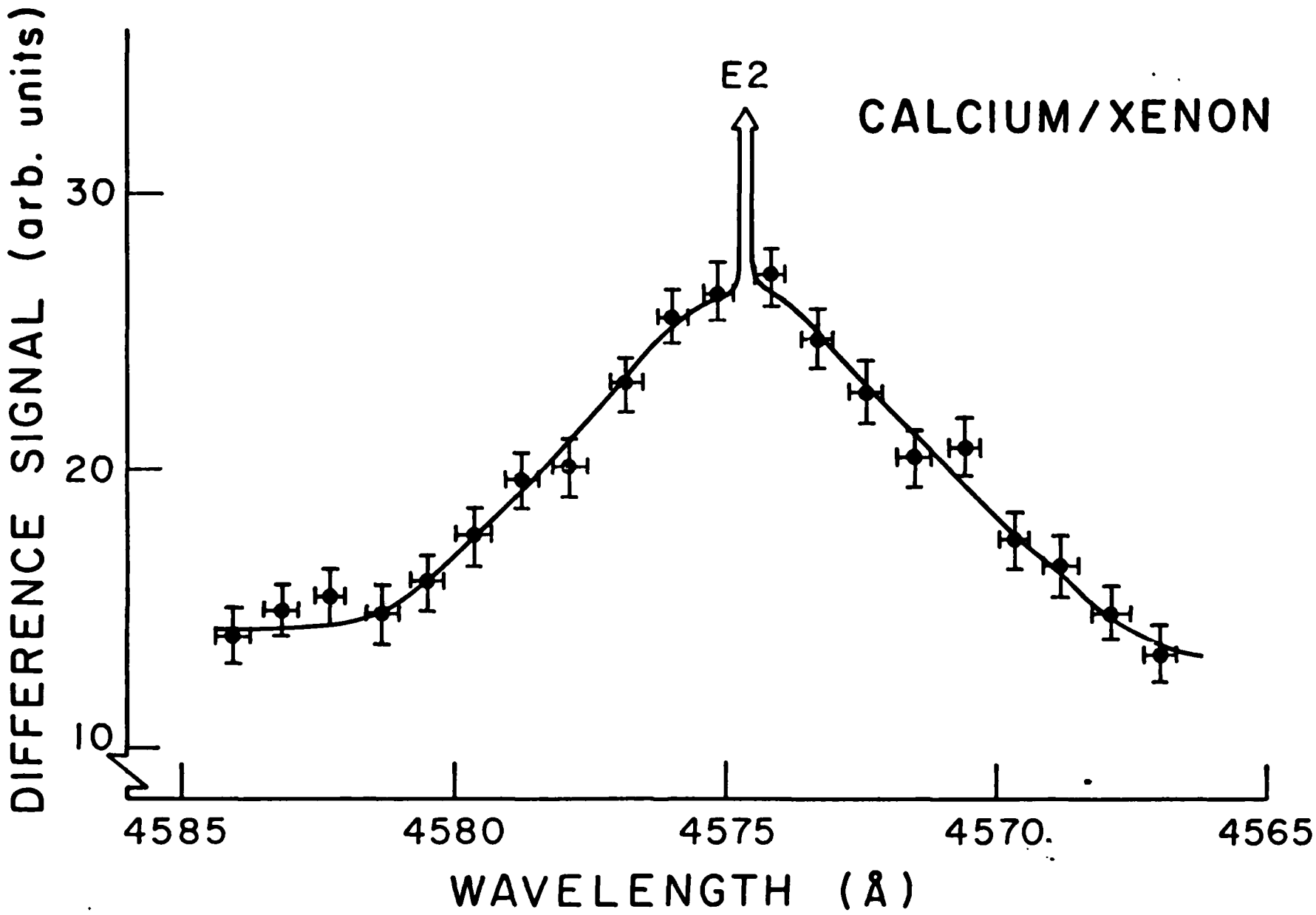

Figure 8.4 The calcium/xenon collisionally induced lineshape data close to the 4575 Angstom E2 transition.

At 500τ of Xenon buffer gas pressure this was the only detection scheme we could devise to yield data.

However, an alternative approach could be tried. Using the approximate effective rate constant for the $^1P_1 \rightarrow {}^3P_J^o$ decay quoted by Wright and Balling, and associating the rate limiting step with the $^1D_2 \rightarrow {}^3D_J$ collisional transfer, it is straightforward to show that lifetime associated with the collisional loss of $^1D_2$ states becomes comparable to the laser pulse duration at a buffer gas pressure of some 50τ. At these lower pressures the original blue/green laser detection scheme should once again become operable. This indeed proved to be the case. At 625°C/650°C finger/cell temperatures; at 50τ guffer gas pressure; the lineshape for the Ca/Xe collisionally induced signal is plotted in figure 8.3. Due to the large collisionally redistributed Ca $^1P_1^o$ signal (of the same order of magnitude as the Ca $^1D_2$ collisionally induced signal) only the difference between the signals due to the blue and green laser combination and the blue laser along is plotted. Since the number of excitations into the Ca/Xe transient molecule is proportional to Xenon pressure, the overall signal levels seen in this experiment dropped by a factor of ten from those used to derive the Ca/He and Ca/Ne data. Computer logging of the data became essential.

Each point is the result of the subtraction of two 401 data point sets. The error bars are some 5 → 10% of the observed difference signal. In this data we see two distinct features - the molecular component contributing to the large blue and weak red wings extending to detunings of some kT/ħ and a component that decreases in importance with increasing detuning around the Ca 4575 Å E2 line. This feature may be explained in terms of a perturbative expansion in terms of adiabatic, time dependent wavefunctions connecting asymptotically to atomic orbitals. It is such regions as this that have

prompted the most comprehensive theoretical investigations into collisionally induced phenomena, and we plot this region in more detial in figure 8.4. The pedestal due to the molecular component has been subtracted off. The horizontal error bars reflect the accuracy to which we may set the blue dye laser frequency. Again 401 data point sets were used and the cell conditions were unchanged with respect to figure 8.3.

Our experience with the improved data collecting equipment used in this set of experiments indicates that the major uncertainty in the data plotted in figures 3 to 6 is due to the drift in signal intensity as a function of time. The Ca/He and Ca/Ne data sets took roughly one laboratory hour to acquire, and the Ca/Xe data sets some two laboratory hours. A 10% drift in signal intensity per hour was observed, and this was corrected for by linear interpolation. This drift is due to the poor long-time stability of our Nd:YAG dye pumping laser. Since the drift in the Nd:YAG laser intensity may not have been uniform in time some regions of our spectra may be subject to a 5% systematic error.

In this section we present data for Ca/Ne, Ca/He and Ca/Xe collision partners. We note that only the Ca/Xe data possess structure that is readily accessible to explanation in terms of quantitative theory at present. It is interesting that we can observe the effects of collisional transfer out of the $^1D_2$ states into the triplet ^3D_J manifold. We are currently undertaking experiments designed to measure the cross sections for collisions $^1D_2$ destruction for the calcium/rare gas collision complexes.

9. Conclusions and Further Work

During the contract period a variety of theoretical and experimental investigations have been successfully undertaken. The description of

collisionally induced transitions is now well advanced, and the extension to include intracollisional coherence velocity changing effects is clear. It is possible to enhance electronic energy transfer collision cross sections by factors of up to one thousand by using a strong laser to bring dressed levels into resonance. Based on experiments on tagged particle diffusion, experiments have been designed and successfully completed investigating the effect of collisions on forbidden lines. These experiments have pioneered a new technique from which non-equilibrium transport phenomena may be measured. Well-isolated spin-forbidden transitions exhibit negligible collisional enhancement of oscillator strength, although spin allowed electric quadrupole transitions may be easily enhanced. This is because the collision process is electrostatic to first order and can take away arbitrary amounts of angular momentum. Interesting collisional induced absorption data has been measured for these spin allowed transitions.

Clearly we feel it important to extend the investigations of collisionally induced processes both theoretically and experimentally. Of prime interest is the prospect of observing velocity changing collisions in the ground state of a radiator species, and indirectly testing the one interacting level approximation. Extension of these ideas to other atoms and molecules will yield additional insight into a fascinating physical process.

10. References

1. W. A. Molander, M. Belsley, A. Streater and K. Burnett, Phys. Rev. A 29, 1548 (1984).
2. G. Kintz and J. Cooper (unpublished work).
3. J. P. Hansen and I. R. McDonald, Theory of Simple Liquids (Academic Press, New York, 1976).

4. R. Desai, J. Chem. Phys. 44, 77 (1966).

5. L. Groome, J. Dufty and M. Lindenfeld, Phys. Rev. A 19, 304 (1979).

6. G. K. Oertel and L. P. Shomo, Tables for the Calculation of Radial Multipole Matrix Elements by the Coulomb Approximation, Astrophys. J. Suppl. 16, 175 (1968).

7. J. P. Boon and S. Yip, Molecular Hydrodynamics (McGraw-Hill, New York, 1980).

8. F. Baas, P. Oudeman, H. Knapp, and J. Beenaker, Physica 89, A 73 (1977).

9. D. Beysen, Y. Garrabos and G. Zalczer, Phys. Rev. Lett. 45, 403 (1980); H. Kiefte, M. Clouter, and R. Penny, Phys. Rev. B 30, 4017 (1984).

10. R. J.Malins and D. J. Benard, Chem. Phys. Lett. 74, 321 (1980).

11. P. S. Furcinitti, L. C. Balling, and J. J. Wright, Phys. Lett. 53A, 1, 75 (1975).

12. D. Husain and J. Schifino, J. Chem. Soc. Faraday Trans. 2 79, 1265 (1983).

13. D. Husain and J. Schifino, J. Chem. Soc. Faraday Trans. 2 79, 1677 (1983).

14. Oscillator Strength of $^3P_1$ line estimated from an average of lifetime measurements of 0.34 ms for $^3P_1 \rightarrow {}^1S_0$ optical decay.

15. M. O. Hale, Ph.D. Thesis, University of Colorado (1984). The fine structure changing cross section is essentially hard sphere, and leads to the estimate that for 10 Torr argon, fine structure mixing of the ^3P_J multiplet would be complete after roughly 10 ns.

16. I. Shoshan, N. N. Dannon, and U. P. Oppenheim, J. Appl. Phys. 48, 11, 4495 (1977).

17. C. R. Vidal and J. Cooper, J. Appl. Phys. 40, 3370, (1969).

18. A. Streater, G. Kintz, J. Cooper, A. Santos, K. Burnett, and J. W. Dufty, Phys. Rev. A 34, 1584 (1986).

19. R. Granier, A. Charton, and J. Granier, J. Quant. Spectrosc. Radiat. Transfer 36, 2, 113, (1986).

20. This approach is analogous to that used by Griem in e.g., A. W. Ali and H. R. Griem, Phys. Rev. 140, A1044 (1965).

21. P. D. Kleiber, J. Cooper, K. Burnett, C. V. Kunasz and M. G. Raymer, Phys. Rev. A 27, 291 (1983).

22. T. F. Gallagher, K. A. Safinya, F. Gounand, J. F. Delpech, W. Sandner and R. Kachru, Phys. Rev. A., 25, 4, 1905 (1982).

23. M. J. Seaton, Proc. Phys. Soc. (1962).

24. J. C. Lewis and J. van Kranendonk, Can. J. Phys. 50, 352 (1972).

25. K. Burnett, J. Cooper, R. J. Ballagh, and E. W. Smith, Phys. Rev. A 22, 2005 (1980).

26. R. Garstang, in Atomic and Molecular Processes, edited by D. R. Bates (Academic Press, New York, 1962), p. 1.

27. M. Lapp, Phys. Lett. 23, 523 (1966).

28. K. Ueda, T. Fujimoto, and K. Fukuda, J. Phys. Soc. Japan 49, 1147 (1980).

29. K. Ueda, Y. Ashizawa, and K. Fukuda, J. Phys. Soc. Japan 50, 625 (1981).

30. K. Ueda, Y. Ashizawa, and K. Fukuda, J. Phys. Soc. Japan 50, 1330 (1981).

31. A. Tam, G. Moe, W. Park, and W. Happer, Phys. Rev. Lett. 35, 85 (1975).

32. G. Moe, A. C. Tam, and W. Happer, Phys. Rev. A 14, 349 (1976).

33. A. C. Tam, T. Yabuzaki, S. M. Curry, and W. Happer, Phys. Rev. A 18, 196 (1978).

34. B. Sayer, M. Ferray, and J. Lozingot, J. Phys. B. 12, 227 (1979).

35. B. Sayer, M. Ferray, J. P. Visticot, and J. Lozingot, J. Phys. B 13, 177 (1980).

36. J. G. Eden, B. E. Charrington, and J. T. Verdeyen, IEEE J. Quantum Electron. QE-12, 698 (1976).

37. K. Ueda and K. Fukuda, J. Phys. Chem. 86, 678 (1982).

38. K. Niemax, J. Quant. Spectrosc. Radiat. Transfer 17, 125 (1977).

39. J. R. Murray and C. K. Rhodes, J. Appl. Phys. 47, 5041 (1976).

40. P. S. Julienne, M. Krauss, and W. Stevens, Chem. Phys. Lett. 38, 374 (1976).

41. J. Pascale and J. Vandeplanque, J. Chem. Phys. 60, 2278 (1974).

42. J. Pascale, J. Chem. Phys. 67, 204 (1977).

43. A. Gallagher and T. Holstein, Phys. Rev. A 16, 2413 (1977).

44. G. Alber and J. Cooper, Phys. Rev. A 33, 3084 (1986).

45. J. J. Wright and L. C. Balling, J. Chem. Phys. 73, 4, 1617 (1980).

46. M. Harris, D. R. McHugh, E. L. Lewis, I. Shannon, and M. Zokai, unpublished.

47. See, for example, R. Loudon, The Quantum Theory of Light (Clarendon, Oxford, 1973).

11. Publications and conference abstracts

"Measurement of tagged particle diffusion using delayed two photon absorption," A. Streater, G. Kintz, J. Cooper, K. Burnett and J. W. Duffy, Phys. Rev. A, 34, 2, 1584 (1986).

"Master equation approach to collisionally induced absorption and emission," G. Alber and J. Cooper, Phys. Rev. A 33, 5, 3084 (1986).

"The effect of collisions on forbidden lines," J. Coutts, S. K. Peck, R. Stoner and J. Cooper, J. Appl. Phys. in press.

"Modifying excitation transfer cross sections witn an a.c. Stark effect," J. Coutts, J. Cooper, and K. Burnett, submitted to Optics Letters.

"Intracollisional studies from light scattering," J. Cooper, AFOSR AFWAL Molecular Dynamics and Surface Chemistry Conference, Albuquerque (1984).

"The effect of collisions on forbidden lines," J. Coutts and J. Cooper AFOSR Contractor's Conference, Boston (1986).

"Collisional effects on forbidden lines," J. Coutts, S. K. Peck and J. Cooper, ICPEAC, Brighton (1987).

"Modification of excitation transfer collision cross sections with an a.c. Stark effect," J. Coutts, J. Cooper, and K. Burnett

"Modification of electronic excitation transfer cross sections with strong optical fields," J. Coutts, J. Cooper and K. Burnett, "Collisions in strong fields 2" Royal Holloway and Bedford New College, Egham (1987).

"Collision induced absorption in the calcium rare gas complex near 4575 angstroms," J. Coutts, S. K. Peck and J. Cooper, ILS III, Atlantic City (1987).

12. The people involved in this contract

The staff involved in this contract as designated principal investigator have been Dr. K. Burnett (1983-84), Dr. J. Cooper (1984-86) and Dr. J. Coutts (1986-87), during the leave of absence of Dr. Cooper at the University of Otago, New Zealand. The students who have been involved as research assistants have been G. Kintz, M. Belsely, R. Stoner and S. K. Peck.

END

JAN.

1988

DTIC